

Mechanisms of Chemotropism in Fungi: *Saccharomyces cerevisiae* as a Model

by

Manuella Rossette Clark-Cotton

Department of Cell Biology
Duke University

Date: _____

Approved:

Daniel J. Lew, Supervisor

Stefano Di Talia

Steve Haase

Terry Lechler

Christopher Nicchitta

Dissertation submitted in partial fulfillment of
the requirements for the degree of Doctor
of Philosophy in the Department of
Cell Biology in the Graduate School
of Duke University

2021

ABSTRACT

Mechanisms of Chemotropism in Fungi: *Saccharomyces cerevisiae* as a Model

by

Manuella Rossette Clark-Cotton

Department of Cell Biology
Duke University

Date: _____

Approved:

Daniel J. Lew, Supervisor

Stefano Di Talia

Steve Haase

Terry Lechler

Christopher Nicchitta

An abstract of a dissertation submitted in partial
fulfillment of the requirements for the degree
of Doctor of Philosophy in the Department of
Cell Biology in the Graduate School of
Duke University

2021

Copyright by
Manuella Rossette Clark-Cotton
2021

Abstract

Budding yeast decode pheromone gradients to locate mating partners, providing a model of chemotropism in fungi. How yeast polarize toward a single partner in crowded environments is unclear. Initially, cells often polarize in unproductive directions, but then they relocate the polarity site until two partners' polarity sites align, whereupon the cells "commit" to each other by stabilizing polarity to promote fusion. Using live-cell fluorescence microscopy, computational modeling, and quantitative autocorrelation analyses, I address the role of the early mobile polarity sites, finding that commitment by either partner failed if just one partner was defective in generating, orienting, or stabilizing its mobile polarity sites. Mobile polarity sites were enriched for pheromone receptors and G proteins, suggesting that such sites engage in an exploratory search of the local pheromone landscape, stabilizing only when they detect elevated pheromone levels. Mobile polarity sites were also enriched for pheromone secretion factors, and simulations suggest that only focal secretion at polarity sites would produce high pheromone concentrations at the partner's polarity site, triggering commitment.

Dedication

This dissertation is dedicated to the people who have given me all the things I love most:

The grandfathers I never knew, but who, along with our grandmothers, gave us the place that we all call home;

Grandma, who gave me my first music lessons;

Mama Pauline, who taught me to read;

My Uncle Mac, who 60 years ago sacrificed his young adulthood, over and over, so that someone like me could someday do something like this;

My three brothers Lauwyn, San, and Dion, the only people who share and understand my childhood memories;

My Daddy, who taught me to vote, ask any question of any person, and cultivate, express, and defend my own opinions;

My Mama, who taught me to cook, love biology, tell our family's stories, and sing alto;

And Yaya, the family's next-generation scientist.

Contents

Abstract	iv
List of Figures	x
Acknowledgements	xii
1. Introduction	1
1.1 Overview of mating in fungi	1
1.1.1 Challenges for cell-cell fusion	2
1.1.1.1 Proximity	3
1.1.1.2 Orientation of growth	3
1.1.1.3 Timing and orientation of cell wall degradation	4
1.1.2 Fungi communicate with chemoattractants	5
1.2 Overview of chemotropic growth in fungi	6
1.2.1 Polarized growth can be triggered by pheromones	6
1.2.2 Pheromones can direct polarized growth toward a partner	8
1.3 Chemical signals promote varieties of chemotropic growth	10
1.3.1 Chemotropism between different cell types	10
1.3.1.1 Bilateral heterothallic mating	10
1.3.1.2 Unilateral heterothallic mating	12
1.3.2 Chemotropism in clonal populations	12
1.3.2.1 Mycelial network formation	12
1.4 Chemical signals also promote non-chemotropic growth	14

1.4.1 Pheromones can trigger polarized growth in clonal populations	14
1.4.1.1 Homothallic (unisexual) mating.....	14
1.5 Models of chemotropic growth.....	17
1.5.1 Spatial sensing model.....	17
1.5.1.1 Molecular “noise”	19
1.5.1.2 Gradient steepness	20
1.5.1.3 Signal complexity	20
1.5.2 Dynamic polarization models	22
2. Exploratory polarization facilitates mating in <i>Saccharomyces cerevisiae</i>	30
2.1 Introduction.....	30
2.2 Results	36
2.2.1 Pheromone sensing and secretion are enriched at transient polarity sites.....	36
2.2.2 Simulating the pheromone landscape experienced by mating cells.....	38
2.2.3 Wildtype cells fail to commit to constitutively indecisive partners	45
2.2.4 Behavior of wildtype cells mixed with prematurely committed partners.....	51
2.2.5 Wildtype cells fail to commit to partners that lack polarity sites	55
2.3 Discussion.....	62
2.3.1 Exploratory polarization underlies partner selection in yeast mating.....	62
2.3.2 Re-evaluating the pheromone landscape of mating cells	64
2.3.3 Advantages of exploratory polarization.....	66
3. Materials and methods.....	68
3.1 Yeast strains and plasmids	68

3.2 Live-cell microscopy.....	70
3.3 Scoring colocalization of Ste2, Ste4, Ste6, and Sec4 with Bem1.....	72
3.4 Mating efficiency	73
3.5 Budding index.....	73
3.6 Halo assays to measure pheromone secretion	74
3.7 Spatial autocorrelation analysis	74
3.8 Calculation of pheromone concentrations expected for global and local secreting cells.....	76
3.9 Simulations of pheromone landscape for two touching cells.....	77
3.10 Analysis of particle-based pheromone simulations	79
3.11 Yeast and plasmid strains and genotypes.....	81
4. Conclusions.....	84
4.1 Conclusions	84
4.2 Future directions.....	85
4.2.1 How do two polarity sites become aligned?	85
4.2.2 Is polarized sensing critical for chemotropism?	86
4.2.3 How does concentrated pheromone raise MAPK levels?.....	87
4.2.4 Does the presence of the Ras-GTPase Rsr1 help or confuse cells during mating?	88
References	89
Biography.....	102

List of Tables

Table 1: Yeast strains and genotypes	81
Table 2: Plasmid strains and genotypes	83

List of Figures

Figure 1: Two distant fungal cells under turgor pressure must locate and grow toward each other, and then fuse without lysing.	5
Figure 2: Fungal communication systems link pheromone sensing to polarity establishment and trigger polarized growth.	8
Figure 3: Cdc42 directs up-gradient growth.	9
Figure 4: Polarized growth during heterothallic mating in three fungi.	11
Figure 5: Pheromone landscapes encountered by yeast cells.	32
Figure 6: Localization of pheromone secretion, sensing, and signaling proteins during the indecisive period.	38
Figure 7: Cell behavior during the indecisive period.	39
Figure 8: Simulations of the pheromone receiver's landscape for two touching cells.	42
Figure 9: Validation of the pheromone simulations and additional detail.	43
Figure 10: Spatial autocorrelation metric.	47
Figure 11: Wildtype cells do not commit to mutants with constitutively mobile polarity sites.	49
Figure 12: Wildtype cells do not commit to partners with constitutively mobile polarity sites, regardless of mating type.	51
Figure 13: Wildtype and <i>cdc24-m1 rsr1Δ</i> mutants secrete similar amounts of pheromones.	52
Figure 14: Mating in "pheromone confusion" conditions.	55
Figure 15: Behavior of <i>cdc24-4^{ts} ste20^{ΔCRIB}</i> mutants in mating mixes.	57
Figure 16: Wildtype cells do not commit to unpolarized partners.	59
Figure 17: Threshold determination for spatial autocorrelation at 35°C.	60

Figure 18: Overexpression of membrane-targeted Cdc24 blocks polarization..... 62

Acknowledgements

Thanks to all of the people who made this work possible:

Nick Henderson for microscopy of the unpolarized mutants; Tim Elston and Mike Pablo for computational modeling; Debraj Ghose for conceiving, developing, troubleshooting, and updating the spatial autocorrelation algorithm;

Nick, Debraj, and Katie Jacobs for countless discussions of models, data, analysis strategies, papers, and all things yeast chemotropism and mating;

Yasheng Gao for troubleshooting problems with the microscope;

Allie McClure for supportive mentoring during my first year;

Debraj and Christine Daniels for taking walks and calls, talking and listening;

Christine, Delisa Clay, Dionna Gamble, and Nicole Solomon for giving me a community of Black female scientists at Duke;

Duke Chapel and the Duke Chapel Choir, for giving me a place to sing;

Dwayne Wise, the first scientist who understood my rural Southern background;

Vince Dionne, who told me that I should be in graduate school;

The Howard Hughes Medical Institute Gilliam Fellowship Program and the Burroughs Wellcome Fund Graduate Diversity Enrichment Program;

And Danny Lew, for his always critical mind and always honest feedback, for indulging my love of writing and reading stuff at the last minute (!), for believing in my intellect, and for teaching me how to think.

1. Introduction

1.1 Overview of mating in fungi

Fungi inhabit an enormous diversity of biological niches and exist in a wide assortment of relationships with other organisms. While some interactions benefit the host (e.g. symbiotic mycorrhizal fungi that promote nutrient uptake in plants) (Rasmann et al., 2017; Smith and Read, 2008; Tedersoo et al., 2020), fungal parasites and pathogens can cause severe plant, animal, and human disease (Doehlemann et al., 2017; Fones et al., 2017; Köhler et al., 2017), making fungi significant industrially, agriculturally, and medically (Konopka et al., 2019).

Within the subkingdom Dikarya, which comprises the subphyla Ascomycota and Basidiomycota, the fungal life cycle is characterized by two distinct stages: a unicellular **yeast** and/or a **filamentous** hyphal mycelium. Depending on the fungus and environmental conditions, yeast may proliferate as haploids or mate to form diploids. In many fungi, yeast can also fuse and differentiate into filamentous forms. These cells can either proliferate as hyphal forms or sporulate, producing more yeast. A mycelium may increase its network connections by fusing hyphal branches (Bennett and Turgeon, 2016; Coelho et al., 2017).

For infectious species, pathogenicity is often linked to these life cycle transitions. For example, the plant smut *Ustilago maydis* is uninfecious as a yeast, but pathogenic as hyphae, while animal pathogens like *Cryptococcus* spp. are infectious primarily as yeasts

(Morrow and Fraser, 2009). Furthermore, adaptation to changing environmental conditions may trigger life cycle transitions. For example, nutrient deprivation and desiccation induce mating and sporulation in *C. neoformans*. A range of triggers, including nutrient deprivation and host-derived signals, cause the yeast form of the opportunistic human pathogen *Candida albicans* to switch to hyphal growth, promoting infection (Arkowitz and Bassilana, 2019). Additionally, through mating, fungi may adapt over generations to become more virulent, inhabit new niches, or respond to evolving host conditions (Wallen and Perlin, 2018). Humans are believed to be protected against infection from most fungi, in part, because they are not adapted to live at our body temperatures. However, as climate change increases ambient temperatures and fungi adapt to those changes, humans may face increasing threats from emerging pathogenic fungi (Casadevall, 2019).

In summary, many fungal life cycle transitions require cell-cell fusion. Mating, frequently an intermediate step in sporulation, requires cell-cell fusion. The transition from yeast to hyphae may involve cell-cell fusion, as does mycelium expansion through hyphal fusion. Therefore, understanding these pathogenic processes requires insight into the general principles by which fungal cells fuse with each other.

1.1.1 Challenges for cell-cell fusion

The typical fungal plasma membrane is surrounded by a cell wall. Fungal cells can reshape their walls by trafficking cell wall-remodeling enzymes to their surface

through vesicle-mediated secretion. When vesicle delivery is restricted to a small site on the cortex, the cell wall is slowly remodeled. In this way, the cell can change its morphology and grow in a polarized fashion (Pruyne et al., 2004a; Pruyne et al., 2004b).

Polarized secretion can also degrade the cell wall. Degrading the cell wall entails a hazard: the presence of a wall creates turgor pressure internally, and penetrating the wall to expose the plasma membrane would cause cell lysis (Levin, 2011). Furthermore, both directed growth and cell wall degradation occur through polarized secretion, requiring the cell to carefully regulate when and where each process occurs. In this section, I discuss the problems of **proximity**, **orientation**, and **timing** associated with remodeling or degrading the cell wall during fusion and the strategies cells use to manage these difficulties.

1.1.1.1 Proximity

Two cells can only fuse if they are touching each other. Walled cells are immotile, which means that fungi can either 1) fuse with nearby partners; or 2) have a mechanism for closing the distance between two cells. Indeed, live-cell imaging has demonstrated that budding yeast several μm apart can grow toward each other until they touch, and that this sort of polarized growth can enable mating (Suchkov et al., 2010).

1.1.1.2 Orientation of growth

Polarized growth allows two distant cells to touch each other and fuse, but polarized growth could be either randomly directed or oriented toward a partner. If the

former were true, then mating would be quite haphazard, occurring between cells that grow into each other by chance. However, if the latter, then there would be a mechanism by which at least one cell could locate, and grow toward, the other.

1.1.1.3 Timing and orientation of cell wall degradation

Polarized secretion delivers both cell wall-degrading hydrolases and cell wall-building synthases to the cortex. Balanced delivery of hydrolases and synthases produces cell wall remodeling and growth, but if more degradation than synthesis occurs, the cell wall becomes thinner and can be degraded. Remodeling modifies the wall without penetrating it, and if secretion is polarized, remodeling changes the cell's morphology (Lesage and Bussey, 2006). The cell wall is reshaped but not penetrated, and remodeling can be safely performed without the threat of lysis. However, if a cell degrades its wall, exposing the plasma membrane to the extracellular environment, it will lyse. This can be avoided by switching to cell wall degradation only after juxtaposition to a partner. If two cells remodel their walls where tightly apposed, the plasma membranes become exposed to each other but the cell's interior remains protected by a common wall surrounding the prezygote (Gammie et al., 1998). Juxtaposition is protective only if the two cells also degrade their walls along a common axis. Cells that fail to align cell wall degradation with the partner will lyse.

In summary, in order to fuse, two cells must solve problems of proximity, orientation, and timing. If the cells are already juxtaposed or stochastically encounter

each other, then the proximity problem is solved. Such a strategy might work well in crowded conditions but would be inefficient in low-density populations. A more efficient strategy would allow one or both cells to find the other and execute directed growth. Once aligned, the cells could safely degrade their cell walls and fuse their plasma membranes. Critically, the cells must identify a common axis of fusion to minimize the threat of lysis (**Figure 1**). Therefore, the two cells need a sophisticated communication system to coordinate the timing and orientation of cell wall remodeling and degradation.

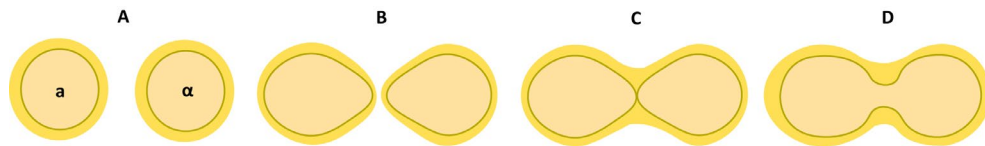


Figure 1: Two distant fungal cells under turgor pressure must locate and grow toward each other, and then fuse without lysing. (A) Each cell is surrounded by a cell wall (gold) that must be degraded while juxtaposed to the partner, to allow the underlying plasma membranes (green) to fuse. (B) Cell wall remodeling produces polarized growth by both cells, bringing them into juxtaposition. (C) Cell wall degradation along a common axis aligns the plasma membranes while protecting the cells from lysis. (D) The membranes fuse at the point of contact, creating a fusion pore for cytoplasmic mixing.

1.1.2 Fungi communicate with chemoattractants

The best-studied cell-cell communication system in fungi mediates mating in *Saccharomyces cerevisiae* and its distant ascomycete relative *Schizosaccharomyces pombe*, where polarized growth is guided by diffusible chemoattractants called pheromones (Dohlman and Thorner, 2001; Martin, 2019). Many elements of pheromone-based guidance, or chemotropism, appear to be conserved throughout the phylum. However,

it is perhaps unsurprising that some elements of pheromone guidance have evolved to function in a variety of additional processes requiring cell-cell fusion, including colony formation, hyphal growth, and even host infection (Wallen and Perlin, 2018). **How do chemoattractants trigger such diverse varieties of cell-cell fusion?**

I begin with an overview of pheromone-based fungal communication systems. Then, I discuss a variety of cell-cell fusion processes which appear to be initiated by chemoattractants. Next, I evaluate several models of fungal chemotropism, including a model of chemotropic and non-chemotropic growth that emerges from recent studies of model fungi. I conclude with a description of the current work.

1.2 Overview of chemotropic growth in fungi

1.2.1 Polarized growth can be triggered by pheromones

Small peptides called pheromones mediate communication between potential mating partners in *S. cerevisiae* (budding yeast) and *S. pombe* (fission yeast). Haploid budding and fission yeast exist in two mating types, and each mating type produces a pheromone that binds G protein-coupled receptors (GPCRs) on the surface of the opposite mating type. Pheromone-receptor binding triggers intracellular signaling modules, typically MAPK pathways, which arrest the cell cycle, activate transcription factors, and upregulate mating-specific genes (**Figure 2**). Pheromone binding also promotes polarized growth through the regulation of Rho-family GTPases. Their activators, guanine exchange factors (GEFs), promote GDP-GTP exchange, converting these

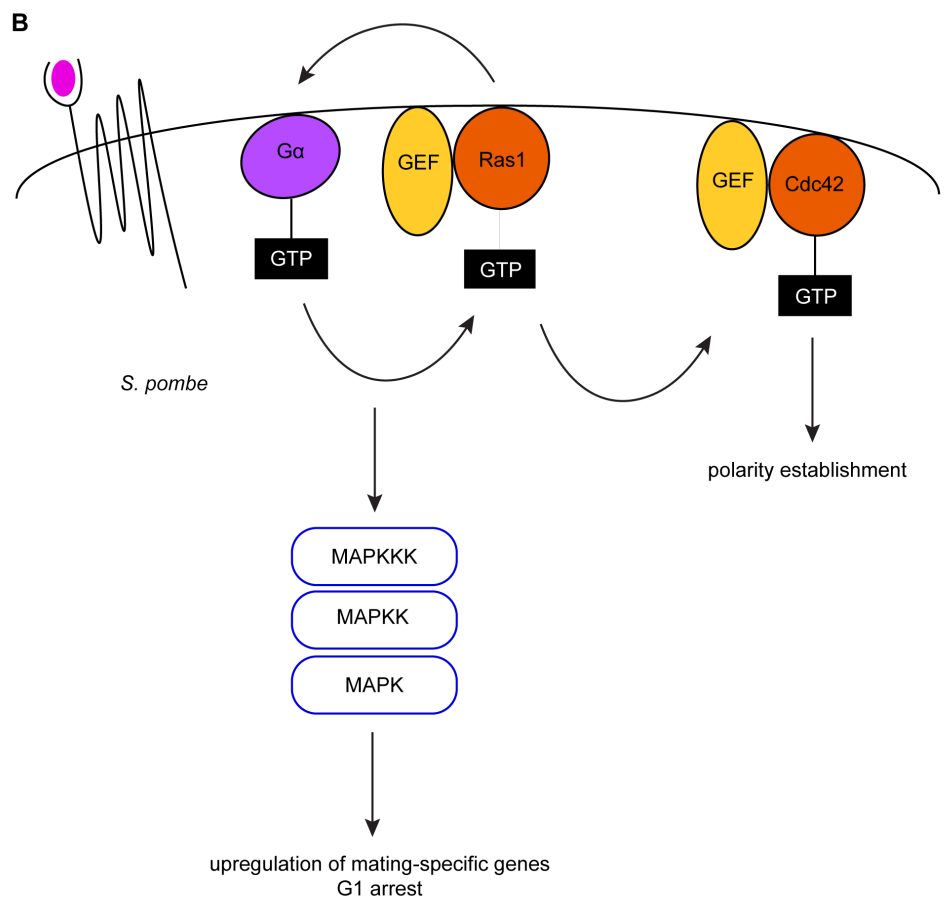
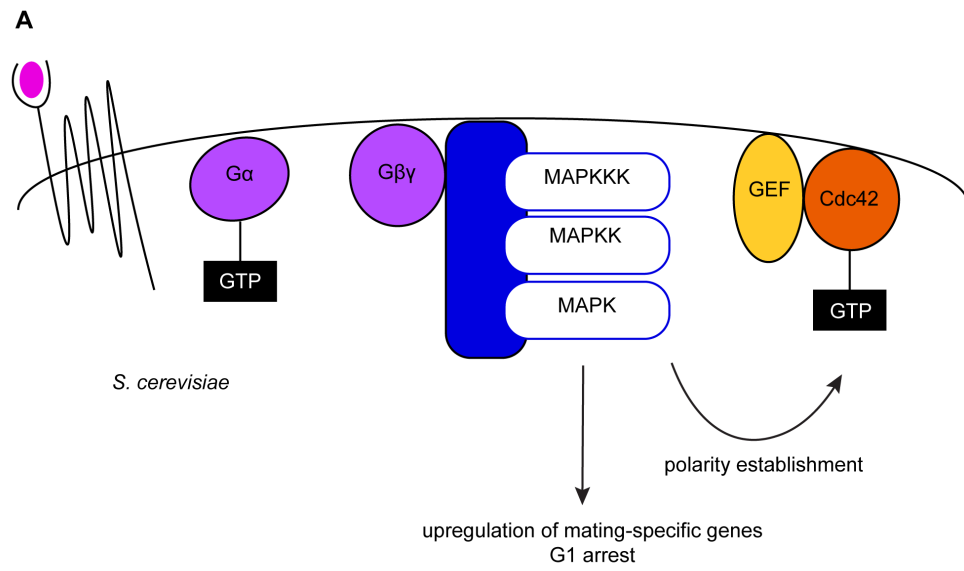


Figure 2: Fungal communication systems link pheromone sensing to polarity establishment and trigger polarized growth. Key components: pheromones, G protein-coupled receptors, G proteins, MAPK cascades, and GTPase modules. (A) In *S. cerevisiae*, pheromone binding activates the G $\beta\gamma$ subunit, which triggers the MAPK cascade and also promotes polarity establishment (Pryciak and Huntress, 1998). (B) In *S. pombe*, G α is thought to promote MAPK activation in concert with a Ras-GTPase (Ras1), while a Rho-GTPase (Cdc42) regulates polarity establishment (Bauman and Albright, 1998; Bendezu and Martin, 2013; Fukui and Yamamoto, 1988; Nadin-Davis and Nasim, 1990; Ozoe et al., 2002; Wang et al., 1991).

GTPases to their GTP-bound, active form. Effectors of active Rho-GTPases promote cytoskeletal reorganization that directs polarized growth (Dohlman and Thorner, 2001; Martin, 2019; Merlini et al., 2013).

Polarized growth triggered by the pheromone response pathway does require pheromone but *does not* require a spatially-graded pheromone signal. *a*-cells treated with uniform, concentrated exogenous α -factor will grow in a polarized manner near the site of the most recent bud emergence (Madden and Snyder, 1992). Therefore, the processes of directional sensing and polarized growth are separable.

1.2.2 Pheromones can direct polarized growth toward a partner

For a cell seeking a mate, the goal of polarized growth is not simply polarized growth, but growth directed toward, and eventual juxtaposition with, a mating partner.

How does a cell direct polarized growth toward a partner?

Studies of *S. cerevisiae* provided insight into the pathway required for polarized growth toward a mating partner (**Figure 3**). The Rho-GTPase Cdc42 can be polarized

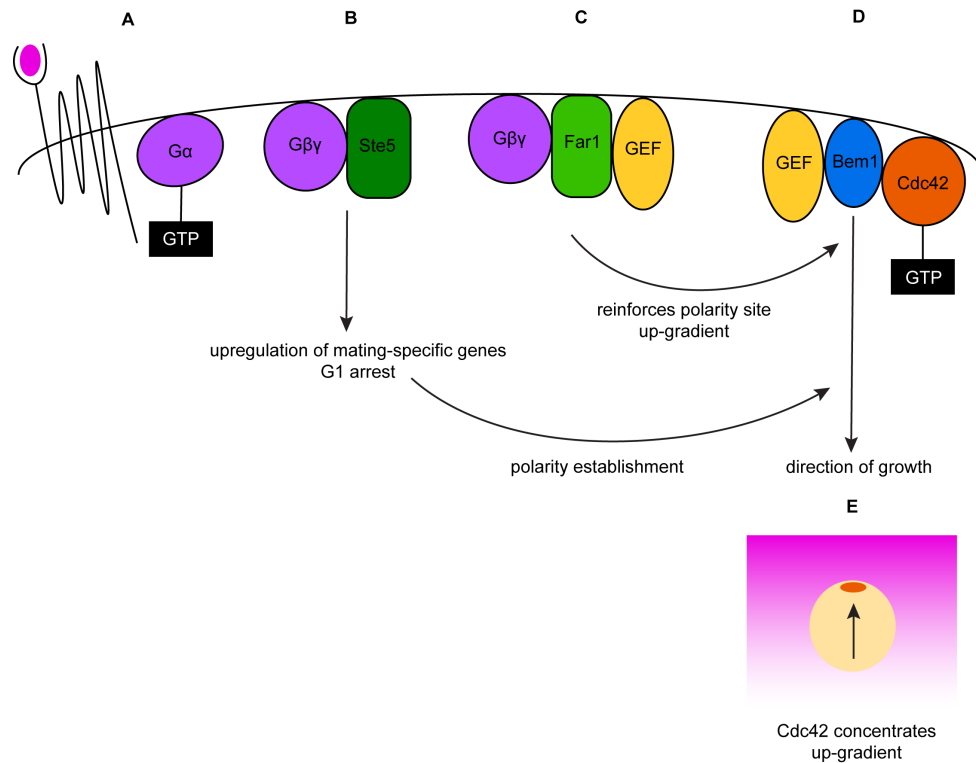


Figure 3: Cdc42 directs up-gradient growth. (A) Pheromone-receptor binding activates $G\beta\gamma$, which recruits (B) the MAPK scaffold Ste5 and (C) the related scaffold Far1. MAPK activation (not shown) promotes G1 arrest and the mating-specific transcription. Far1 forms a complex with $G\beta\gamma$ and the GEF for Cdc42. (D) The GEF also binds Bem1 and the Rho-GTPase Cdc42, promoting its active form, Cdc42-GTP and triggering polarized growth. Therefore, the Far1 pathway couples pheromone sensing to the direction of polarized growth during mating in *S. cerevisiae*, (E) concentrating Cdc42-GTP up the pheromone gradient.

through its interactions with the scaffold protein Bem1, which also binds the GEF for Cdc42 (Irazoqui et al., 2003). Through this Bem1 complex, the GEF converts inactive Cdc42-GDP to active Cdc42-GTP, reinforcing Cdc42 activity by positive feedback and locally concentrating active polarity proteins (Johnson et al., 2011; Kozubowski et al., 2008). Effectors of Cdc42-GTP reorganize the actin cytoskeleton to promote polarized growth where Cdc42-GTP is concentrated (Pruyne et al., 2004a; Pruyne et al., 2004b).

As GPCRs, pheromone receptors are associated with the G proteins $G\alpha$ and $G\beta\gamma$. When activated by pheromone binding, $G\beta\gamma$ recruits the MAPK scaffold Ste5 and also forms a complex with the GEF and a third protein, Far1, locally reinforcing Cdc42-GTP where the pheromone concentration is greater (Butty et al., 1998; Nern and Arkowitz, 1999). Therefore, the site of positive feedback (and polarized growth) is influenced by the spatial distribution of the pheromone signal (Nern and Arkowitz, 1998; Valtz et al., 1995).

1.3 Chemical signals promote varieties of chemotropic growth

1.3.1 Chemotropism between different cell types

1.3.1.1 Bilateral heterothallic mating

The best-known examples of pheromone guidance occur between two mating types (“heterothallism”) and involve two pheromones, as in the budding yeast *S. cerevisiae* and the fission yeast *S. pombe* (Martin, 2019; Merlini et al., 2013). In budding yeast, **a**-cells secrete a-pheromone (“a-factor”) and display receptors that bind α -pheromone (“ α -factor”). Conversely, α -cells secrete α -factor and bind a-factor. Similarly, haploid fission yeast are either mating type h^+ (secreting P-factor and displaying M-factor receptors) or h^- (producing M-factor and P-factor receptors). Therefore, both mating types respond to the opposite cell type but not to their own pheromones. Bilateral polarized growth by each partner facilitates juxtaposition, and the point of contact defines the fusion axis (**Figures 4A** and **4B**).

Although their ploidies differ in the wild (*S. pombe* is haploid, *S. cerevisiae* is diploid), the diploid of both yeasts sporulates under starvation. Therefore, when

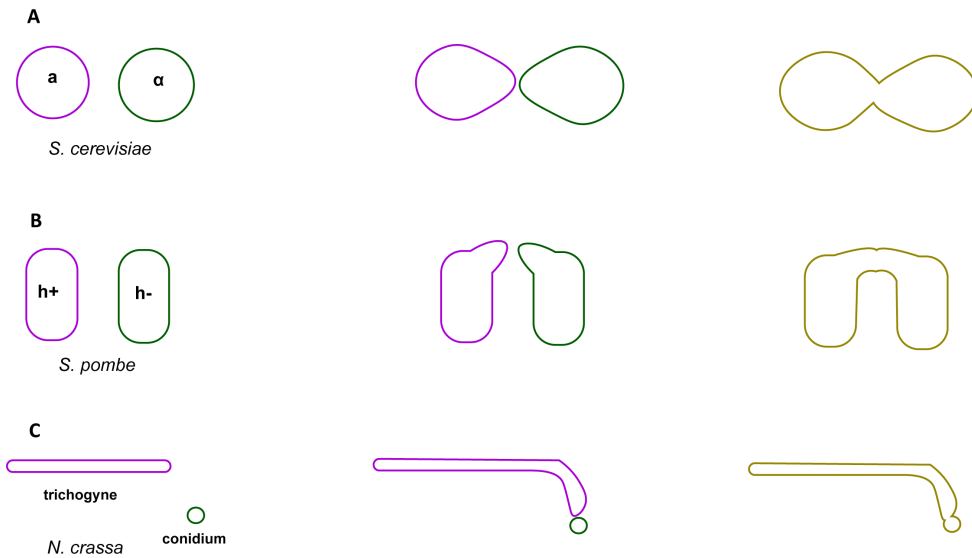


Figure 4: Polarized growth during heterothallic mating in three fungi. (A,B) In *S. cerevisiae* and *S. pombe*, cells of opposite mating type grow toward each other and fuse. (C) In *N. crassa*, the two mating types develop different morphologies, and only the female structure exhibits polarized growth.

starved, the diploid budding yeast sporulates, and the haploid fission yeast mates, then sporulates. However, elements of the pheromone response pathway are similar in both. Both have two pheromones, two GPCRs with associated G proteins, a MAPK cascade, transcription factors that promote the upregulation of mating-specific genes, and Rho-GTPases that specify the site of polarized growth (Merlini et al., 2013). While both are ascomycetes, *S. cerevisiae* and *S. pombe* reside in different subphyla (*Saccharomycotina* and *Taphrinomycotina*, respectively) and diverged from their common ancestor more than 330 million years ago (Bennett and Turgeon, 2016). Their use of very similar systems despite

this evolutionary distance suggests that the core elements of the pheromone response pathway might be well-conserved across the phylum.

1.3.1.2 Unilateral heterothallic mating

In *S. cerevisiae* and *S. pombe*, the two mating partners are morphologically indistinguishable, but some fungi exhibit sexual dimorphism, in addition to mating type differences. An example is the filamentous fungus *Neurospora crassa*, which has two mating types (A and a). Each mating type produces a pheromone and a receptor for the cognate pheromone of the opposite mating type. Both mating types can form either “male” (small gamete) or “female” (large gamete) structures. The female trichogyne grows toward the male conidium in a manner that depends on a chemical signal released by the male cell (Kim and Borkovich, 2004; Kim and Borkovich, 2006; Kim et al., 2012) (**Figure 4C**). Reciprocal growth by the conidium has not been reported during mating, so this appears to be an example of unilateral pheromone guidance by the male cell.

1.3.2 Chemotropism in clonal populations

1.3.2.1 Mycelial network formation

While some fungi can branch and septate to form a mycelium, others can form a network by fusing individual cells. In *N. crassa*, a mycelial network is established when vegetative spores called conidia germinate and fuse with each other, forming a hyphal network. Those hyphae can also fuse with each other, further developing the network

and increasing the colony's access to nutrients and water (Herzog et al., 2015). Although two mating types (A and a) exist, they are incompatible as fusion partners during vegetative growth. If an A and a cell fuse during vegetative growth, the fusion product will die. There is no evidence of mating type-switching as found in budding and fission yeast (Glass et al., 1988). Therefore, vegetative cell-cell fusion in *N. crassa* is an example of fusion between genetically identical cells. The examples of cell-cell fusion discussed so far rely on the reciprocal chemoattractant sensing by two partners that make *different* pheromones and *different* receptors. **How could two identical cells locate each other?**

One possibility is that fusion is limited to cells that are already near each other, without the necessity of guidance over a distance. If so, then conidia (also called "germlings") would need some sort of trigger to signal the proximity of a partner, but they would only fuse with cells that were already adjacent to them. However, micromanipulation studies revealed that conidia of the same mating type could reorient hyphal growth toward each other, suggesting directed growth involving a diffusible signal (Roca et al., 2005; Wright et al., 2007).

Live-cell imaging with fluorescent probes demonstrated a striking oscillatory pattern of signaling at the growing hyphal tips of a pair of communicating cells. At one tip is a MAPK complex homologous to the pheromone-responsive pathway in *S. cerevisiae*, and at the other is the protein SO, a scaffold molecule for the cell wall integrity pathway (a surveillance mechanism that regulates the remodeling of the fungal cell

wall) (Levin, 2011). Approximately every four minutes, the localization alternates (Dettmann et al., 2012; Fleissner et al., 2009; Jonkers et al., 2014). Despite the involvement of the MAPK pathway, neither the mating pheromones nor their receptors are necessary for vegetative chemotropic guidance (Kim and Borkovich, 2004; Kim and Borkovich, 2006), suggesting the presence of a novel chemoattractant. Together, these results suggest that these genetically-identical cells of the same mating type find each other by alternately sending and receiving the same signal.

1.4 Chemical signals also promote non-chemotropic growth

1.4.1 Pheromones can trigger polarized growth in clonal populations

Pheromones and other elements of the pheromone response pathway have also been implicated in non-canonical mating between cells of the same mating type.

1.4.1.1 Homothallic (unisexual) mating

In recent decades, studies have revealed that some fungi are capable of primary homothallism, or mating (including meiosis and genetic recombination) between cells of the same mating type (Lin et al., 2005). Note that this is distinct from the secondary homothallism, or “mating-type switching,” that can occur in budding and fission yeasts. In budding yeast, mating type is specified by the *MAT* locus (either *MAT_a* or *MAT_α*). On the same chromosome, each cell also maintains two inactive copies of both *MAT* genes (*HML_α* and *HMR_a*) at heterochromatic loci. Through homologous recombination, an inactive sequence can be copied into the *MAT* locus, thereby causing a cell to adopt

the opposite mating type, producing different pheromones and receptors (Haber, 2012). In organisms that switch mating type, mating can then occur between cells of different mating type.

The basidiomycete *Cryptococcus* can respond to environmental stresses, including nitrogen depletion and water loss (Hull and Heitman, 2002) with a unisexual mating process called “fruiting” (Lin et al., 2005). *Cryptococci* exist in two mating types, but α -cells predominate in clinically relevant isolates and in the wild (Zhao et al., 2019). There is compelling evidence that unisexual mating occurs in the wild, with α - α diploids of *C. neoformans* and *C. gattii* implicated in human and animal infections (Bui et al., 2008; Fraser et al., 2005). In the laboratory, α - α fruiting is triggered by the presence of nearby **a**-cells. Importantly, the **a**-cells do not need to touch the α -cells and can promote fruiting through a diffusible membrane (Wang et al., 2000). Fruiting is also less efficient than mating, requires several weeks of incubation, and appears to occur stochastically in a population (Lin et al., 2005), as might be expected for a process that depends on coincidental encounters between cells, rather than directed growth. These results suggest that a-factor somehow triggers α -cells to fuse with each other through a non-chemotropic process.

Unisexual **a-a** mating has also been reported in *C. albicans*. The first hints came from studies showing that homothallic mating could be induced in single-sex populations (both **a-a** and α - α) by introducing the opposite pheromone into the

environment. In *C. albicans*, a-cells produce some α -factor (Bennett and Johnson, 2006), as well as the α -factor-degrading protease Bar1. Although a-a mating was not detected in wildtype a-cell populations, *bar1* Δ a-cell populations initiated a pheromone response that depended on the α -factor receptor Ste2 and mated, albeit at frequencies much lower than a- α mixtures. Adding α -cells to an a-cell population (or a-cells to an α -cell population) produced a similar unisexual mating outcome (Alby and Bennett, 2011; Alby et al., 2009). Therefore, these cells appeared to be capable of self-mating under conditions that enriched the opposite type of pheromone in the environment. Since wild populations are generally clonal and have intact Bar1, the degree to which this occurs in nature is unclear. However, recent reports that environmental factors, including glucose deprivation and oxidative stress, can trigger a pheromone response and mating in a-a populations suggested physiologically relevant scenarios under which *C. albicans* might undergo unisexual mating (Guan et al., 2019). **How could the presence of the opposite mating type's pheromone trigger mating between cells of the same mating type?**

To analyze this behavior, recall the four problems that fungal cell must solve in order to fuse: proximity, orientation of polarized growth, timing of cell wall degradation, and orientation of fusion. For cells that are sufficiently crowded, proximity is not a problem. If a high concentration of pheromone can trigger polarized but randomly-oriented growth, as noted above in budding yeast, then the presence of the opposite mating type's pheromone in the environment might trigger sufficient growth

to align cells with partners that were some distance away. With such a mechanism, cells would still need to regulate the timing of cell wall degradation (i.e., wait until alignment with a partner to degrade the cell wall) and coordinate the axis of fusion with the partner.

1.5 Models of chemotropic growth

Researchers have advanced several models of directional sensing, for both chemotropism and the related process of movement up a concentration gradient, chemotaxis. Here, I evaluate two key approaches, spatial sensing and dynamic polarization, and the strengths and unresolved questions associated with each.

1.5.1 Spatial sensing model

When starved, unicellular *D. discoideum* aggregate and form a multicellular fruiting body that sporulates. This “swarming” behavior can be recapitulated in the laboratory with a micropipet filled with cAMP: *D. discoideum* move toward the source of the cAMP and aggregate. One possible way to do this is to compare the concentration of chemoattractant at different times, adjusting their path based on this input, as *E. coli* do (Adler, 1975). Studies with exogenous cAMP gradients demonstrated that *D. discoideum* concentrated different proteins on the up- and down-sides of a cAMP gradient. But because they could correctly orient these proteins even when immobilized, scientists concluded that *D. discoideum* can sense a concentration gradient across its diameter

without any temporal input (Artemenko et al., 2014; Cai and Devreotes, 2011; Swaney et al., 2010). This has been dubbed a **spatial sensing model**.

By the late 1980s, researchers recognized the mating process in the genetically tractable yeast *S. cerevisiae* as a model for investigating chemotropism (Cross et al., 1988). Some of the molecular processes underlying chemotropism were known: pheromones secreted by each cell triggered cell cycle arrest and mating-specific gene expression. But these pheromones were also suspected to signal the location of each partner. Two seminal studies of mating under crowded conditions showed that cells were attracted to partners that made pheromone, even if those partners were sterile, but were not enticed by partners deficient in pheromone production (Jackson and Hartwell, 1990a; Jackson and Hartwell, 1990b). These data were interpreted as support for the idea that the cells find a partner by sensing a pheromone gradient. A study showing that a-cells grew up a gradient of exogenous α -factor reinforced this notion (Segall, 1993). Then, mutants impaired in growth up a gradient were identified in a series of studies, and the Far1 pathway required for gradient tracking was described (Butty et al., 1998; Nern and Arkowitz, 1998; Nern and Arkowitz, 1999; Nern and Arkowitz, 2000; Valtz et al., 1995).

Studies suggesting spatial sensing in *Dictyostelium discoideum* influenced models of directional sensing in eukaryotes generally, and experiments conducted in budding yeast were also consistent with spatial sensing. In this model, Far1 links the sensing machinery ($G\beta\gamma$) to polarity proteins (Cdc42 and its GEF Cdc24), which specify the site

of polarized growth through a positive feedback mechanism (Kozubowski et al., 2008). Therefore, a cell encountering a pheromone signal would activate more polarity molecules up-gradient and grow toward the pheromone source (Arkowitz, 1999; Arkowitz, 2009).

While the identification of a specific pathway that allows for growth up-gradient made this model attractive, many questions remained. Below, I discuss each in turn.

1.5.1.1 Molecular “noise”

Chemoattractant systems can be stochastically activated and inactivated (a phenomenon known as “noise”) (Miyanaga et al., 2007). Given that the polarity system operates through a positive feedback loop (Kozubowski et al., 2008), any pheromone signal, not just an up-gradient signal, might be expected to trigger stable polarization. As noted earlier, a-cells treated with uniform, concentrated α -factor grow in a polarized fashion. The site of polarized growth is determined by internal landmarks that specify a bud site during vegetative growth. Through the Ras-GTPase Rsr1, these landmarks can recruit the GEF for Cdc42, in an alternative to the Far1 pathway referred to above. However, a-cells lacking Rsr1 also exhibit polarized growth in concentrated, uniform α -factor. In the absence of a directional pheromone cue or an internal landmark, the cell simply grows in a random direction. Such a system should be error-prone, and reconciling these observations with robust orientation up a gradient is challenging.

1.5.1.2 Gradient steepness

Given an estimated diffusion constant of $150 \mu\text{m}^2/\text{s}$ for α -factor and the small size of a haploid budding yeast cell ($\sim 4 \mu\text{m}$), the gradient across a sensing cell's diameter would be shallow. However, cells can discriminate gradients that are estimated to lead to only a 1-2% difference in receptor occupancy, or a difference of ~ 55 receptors, across their diameter (Lakhani and Elston, 2017; Segall, 1993). It is unclear how an error-prone system, as described above, could reliably discriminate such a small difference.

1.5.1.3 Signal complexity

In discussions of mating, the pheromone environment is usually reduced to one pheromone-emitting α -cell and one nearby pheromone-receiving **a** cell. In this scenario, **a**-cell's task is to determine which way is up-gradient. With a single, stable pheromone source as the founding assumption, many researchers have investigated chemotropism by treating **a**-cells with a stable gradient of α -factor in a microfluidics device. (The chemical properties of α -factor make it infeasible to purify and apply exogenously in the laboratory.) In reality, the pheromone landscape around a cell is complex. This is readily evident if a second α -cell is added to the environment. While it is reasonable that the **a**-cell could discriminate between two α -cells at different distances away from it, a gradient would not help the **a**-cell distinguish between two similarly-distant targets, such as a mother-daughter pair.

Under physiological conditions, cells can encounter scenarios that require them to choose one of two similarly-attractive targets. Following sporulation, four haploid spores (two of each mating type, constituting a “tetrad”) are housed inside an ascus. Although each cell is roughly equidistant to either potential partner, they can successfully mate within the tetrad (Taxis et al., 2005). In the wild, newly-germinated *S. cerevisiae* spores often proliferate for several cycles before mating, forming closely-packed microcolonies of equally-appealing mating partners (McClure et al., 2018).

a-cells also make an α -factor-degrading protease, Bar1, that reshapes the α -factor environment. Exactly how Bar1 changes the α -factor concentration is unknown. When mixed with α -cells at high density, **a**-cells lacking Bar1 exhibit polarized growth that is reminiscent of cells treated with exogenous α -factor. In those conditions, the presence of Bar1 clearly reduces the overall concentration of α -factor. But it might also reshape the local environment around an individual cell, sharpening the local gradient and allowing it to determine the direction of the pheromone source more accurately.

In summary, in the wild, yeast simultaneously encounter multiple, similarly-attractive pheromone sources and constantly reshape the landscape. Therefore, although yeast can accurately sense shallow artificial gradients, and gradient sensing might contribute to chemotropism, it is not obvious how this strategy would be successful in the wild.

1.5.2 Dynamic polarization models

The spatial sensing model was intellectually guided by experiments with **a**-cells exposed to an exogenous gradient of α -factor for several hours, but the development of live-cell imaging techniques with finer time resolution allowed polarization in *S. cerevisiae* to be investigated on a several-minutes time scale. Cdc42 and its effectors concentrate at the site of polarized growth (Arkowitz, 2009), forming a “polarity site.” The scaffold protein Bem1 binds Cdc42 and its GEF during polarization (Irazoqui et al., 2003) (**Figure 3**). Therefore, fluorescent Bem1-GFP or Bem1-tdTomato can be used to visualize the polarity site during pheromone exposure.

When **a**-cells were observed in saturating α -factor, their polarity sites appeared stable, mediating polarized growth that produced a pointed morphology. However, in sub-saturating α -factor, the polarity sites appeared mobile. While polarized growth still occurred, the morphology was blunter. Furthermore, cells that were genetically manipulated to have less mobile polarity sites were less effective at accurately growing up a gradient (Dyer et al., 2013).

As noted earlier, *S. pombe* also has two mating types and a system of pheromones, receptors, MAPK signaling, and a Rho-GTPase polarity regulator that is similar to *S. cerevisiae*'s. In parallel, other researchers conducting live-cell imaging studies in *S. pombe* also demonstrated the presence of mobile polarity sites during mating. These polarity sites could be seen at different places on the cortex over extended

time, in some cases up to 18 hours. Imaging at 15- and 30-second intervals revealed that the proteins can disappear and reappear at different regions of the cortex on very short time scales, suggesting that they are leaving the membrane and being recruited back to different locations, rather than smoothly navigating up-gradient. Cell wall synthases did not localize to the polarity sites during this exploratory period, appearing only once two partners had oriented polarity sites toward each other. These data led to a model in which polarity sites that sense low levels of pheromone explore their environment (often for hours) and execute polarized growth only when they sense sufficiently high pheromone concentrations (Bendezu and Martin, 2013). These critical observations provided the first evidence of mobile polarity sites during the mating process, not only in cells treated with exogenous pheromone.

Together, these data from both budding and fission yeast suggested that mobile polarity sites might be critical for accurate gradient sensing. However, it was also possible that they co-occurred with directional sensing without being functionally important. **How might mobile polarity sites contribute to gradient sensing?**

One possibility arose from earlier experiments showing that the pheromone receptors of **a**-cells concentrate at the tip of a cell during pheromone-induced polarized growth (Suchkov et al., 2010). Recall that Cdc42 also polarizes to the growing tip. Therefore, during stable polarized growth, receptors colocalize with the polarity site. If these receptors colocalize with a mobile polarity site, in a cell that is attempting to

navigate up a pheromone gradient, then the polarity site might function as a mobile “nose.”

As noted earlier, the pheromone receptors are GPCRs with associated heterotrimeric G proteins. When pheromone binds the receptor, $G\beta\gamma$ is activated to trigger a MAPK cascade and reinforce the location of the polarity site where $G\beta\gamma$ is more abundant. Therefore, according to this model, both receptors and $G\beta\gamma$ are co-localized with the mobile Bem1 polarity site during directional sensing. This proposal is particularly intriguing for the starkly different prediction it makes by comparison with a spatial sensing model. While a spatial sensing model assumes that receptors are uniformly distributed around the cell surface, a dynamic polarization model predicts that an unpolarized receptor- $G\beta\gamma$ unit would cause a chemotropism defect. Importantly, if either $G\beta\gamma$ or the receptor were unpolarized, polarized activity would be restricted to the site of the polarized protein. **How could receptors and $G\beta\gamma$ be polarized during the search?**

Recall that effectors of active Cdc42 promote vesicle delivery toward the polarity site. As transmembrane proteins, pheromone receptors would be expected to be trafficked on vesicles. G proteins colocalize with Cdc42 in cells treated with saturating pheromone, i.e., cells with stable polarity sites and polarized growth (Arkowitz, 2009). Data suggest that G proteins and receptors are associated throughout the search process (Strickfaden and Pryciak, 2008), raising the possibility that the receptor- $G\beta\gamma$ unit might

be trafficked together on vesicles. If vesicles delivered receptor-G $\beta\gamma$ complexes to the polarity site, this pair of proteins would together bind pheromone, release G $\beta\gamma$ locally, and reinforce the polarity site's location through the Far1 pathway (**Figure 3**), providing a potential mechanism for stabilizing the polarity site where the pheromone concentration was greater.

In experiments with cells genetically altered to form strong yet mobile polarity sites that could be tracked over time, polarity sites were less mobile in higher vs. lower concentrations of pheromone. Computational modeling suggested that unpolarized G $\beta\gamma$ delivery would not slow polarity site mobility but polarized delivery would. Consistent with this finding, cells genetically manipulated to have both unpolarized G $\beta\gamma$ and unpolarized receptors were unable to slow polarity site wandering. However, those cells also lacked G α , and it is unclear what role, if any, the absence of G α played in their polarity sites' incessant mobility. Furthermore, strong, mobile polarity sites were produced by artificially inducing MAPK (McClure et al., 2015). A second study using cells placed in artificial pheromone gradients reported that mobile polarity sites became better aligned with a pheromone gradient over time (Hegemann et al., 2015).

Although inconclusive, the data from both budding and fission yeast were consistent with a model in which polarity sites act as pheromone-sensitive mobile sensors, promoting mobility when the concentration of pheromone is low and reinforcing the polarity site's location when the concentration is high. Note that this

would be a local sensing strategy, in which the pheromone concentration around the sensor, not the concentration across the cell's diameter, would be critical. But secreted proteins like α -factor and transmembrane proteins like pheromone receptors (and perhaps, their associated G proteins) are delivered to the cell surface by actin-dependent vesicle secretion. These proteins are also known to concentrate at stable polarity sites (Arkowitz, 2009). Therefore, the same mechanism that polarized sensing could also polarize secretion, making the polarity site not only a mobile sensor, but a mobile sensor and secretor. A key question was whether the proteins needed to mediate either local sensing, local secretion, or both colocalized with local polarity sites during their search for a mating partner.

A second live-cell imaging study of fission yeast during mating investigated this issue directly. In mating pairs, the proteins that mediate pheromone secretion and the $G\alpha$ subunit, which activates the MAPK cascade (**Figure 2**), all colocalized with mobile polarity sites during the search for a partner. Although the receptor did not appear to be concentrated at mobile polarity sites, only polarizing $G\alpha$ would be sufficient to localize signaling downstream of the receptor. Computational modeling indicated that both sensing and secretion would need to be polarize to produce efficient mating partner pairing (Merlini et al., 2016). These results were compelling evidence that mobile polarity sites function as roving sensor-secretors. However, no chemotropism pathway

has been identified in fission yeast, so there remained no way to explain how a high concentration of pheromone immobilized polarity sites in *S. pombe*.

Several recent live-cell imaging studies of *S. cerevisiae* demonstrated that budding yeast also form mobile polarity sites, in shallow gradients (Hegemann et al., 2015) and in mating mixes (Henderson et al., 2019; Wang et al., 2019). In cells of both mating type, polarity sites spent a variable indecisive period (from 10 to 120 min) appearing at different locations on the cortex before stably orienting toward one another until fusion. The pattern of MAPK activity during the indecisive period was probed with a MAPK sensor. The coorientation of a pair of polarity sites coincided with a peak in MAPK activity (Henderson et al., 2019).

These data led to the **speed dating model** (fission yeast) and the **exploratory polarization model** (budding yeast), in which each cell establishes mobile polarity sites when they sense low levels of pheromone. These sites explore the cortex, sensing local pheromone levels and secreting concentrated pheromone. When two sites become cooriented, they mutually reinforce each other's location, as each cell senses concentrated pheromone locally (Henderson et al., 2019; Merlini et al., 2016). In budding yeast, the two partners commit within minutes of each other. Reinforcement of the budding yeast polarity site is thought to occur through the Far1 pathway and trigger high MAPK signaling (Henderson et al., 2019). Together, these models offer a unified mechanism of directional sensing based on local sensing and secretion.

However, key questions remain unresolved. First, if the exploratory model is correct, then both pheromone secretion and sensing molecules would be concentrated at mobile polarity sites at some point during the indecisive period. However, these molecules have not been tracked over time with fine time resolution. This analysis would provide insight into when during the search process local sensing and/or secretion might occur.

Second, although mobile polarity sites have been reported by multiple research groups in different experimental settings (low-level uniform pheromone, stable pheromone gradients, and mating mixes) and evolutionarily distant fungi, it remains unclear whether these mobile sites are functionally significant for directional sensing. If they are, then disrupting them would impair commitment to a partner. However, if mobile polarity sites are not necessary for localizing a pheromone source, then cells would be able to commit to a partner even if they are altered or absent.

Third, the data underlying the speed dating and exploratory polarization models suggest that the process occurs bilaterally, but it is unclear whether both partners, or only one, needs to search. If both partners need to be able to search, then a search with one impaired partner would fail. However, if only one needs to search, then a unilateral effort, with one impaired partner, would be successful.

Finally, it has long been observed that **a**-cells treated with concentrated α -factor mate at lower frequencies than cells without exogenous α -factor added. The assumption

was that excess pheromone obscured the directional signal “confused” the **a**-cells (Dorer et al., 1997; Dorer et al., 1995), suggesting that some cells have a less efficient, non-chemotropic mating mechanism.

In this study, I first investigate the colocalization of sensing and secretion molecules with mobile polarity sites. Next, I report simulations of diffusion-mediated changes in the pheromone landscape during mating, showing how local vs. global secretion by one cell affect the concentration of pheromone at sensing cell’s polarity site. Then, I use live-cell fluorescence imaging in budding yeast mutants with altered polarity sites to experimentally test the necessity of mobile sites. Finally, I use live-cell imaging to show how “confused” **a**-cells in concentrated α -factor mate.

2. Exploratory polarization facilitates mating in *Saccharomyces cerevisiae*¹

2.1 Introduction

Directed growth (chemotropism) or movement (chemotaxis) in response to a chemical signal is critical for biological processes including aggregation in *Dictyostelium discoideum* (Nichols et al., 2015), pollen tube growth during plant fertilization (Higashiyama and Takeuchi, 2015), axon guidance during neural development (Bellon and Mann, 2018), and neutrophil migration in the mammalian immune response (Sarris and Sixt, 2015). However, the mechanisms by which cells choose the direction of polarized growth or movement are incompletely understood.

Yeast cells polarize secretion, and hence growth, towards their partners during mating (Merlini et al., 2013). *Saccharomyces cerevisiae* cells of each mating type, **a** and α , secrete pheromones that are sensed by cognate G protein-coupled receptors on cells of the opposite mating type. Pheromone sensing triggers the activation of a MAPK cascade, cell cycle arrest in G1, increased transcription of mating-specific genes, and polarized growth toward the mating partner (Dohlman and Thorner, 2001).

Polarity is directed by the Rho-GTPase Cdc42, which becomes concentrated together with its regulators and effectors at a small region of the cell's cortex to form a

¹ A version of this chapter will be published as Clark-Cotton MR, Henderson NT, Pablo M, Ghose D, Elston TC & Lew DJ. Exploratory polarization facilitates mating partner selection in *Saccharomyces cerevisiae*. *Molecular Biology of the Cell* (in press).

“polarity site” (Park and Bi, 2007). Polarity sites are assembled by a positive feedback mechanism in which active Cdc42-GTP binds the scaffold protein Bem1, promoting the activation of nearby inactive Cdc42-GDP to form a cluster of polarity factors (Johnson et al., 2011; Kozubowski et al., 2008). Formins (effectors of Cdc42) trigger the orientation of actin cables toward the site, promoting delivery of secretory vesicles (Pruyne et al., 2004b).

Yeast cells exposed to a stable pheromone gradient tend to grow up-gradient (Segall, 1993), and stable gradients are often assumed to mediate partner selection (Arkowitz, 1999; Ismael and Stone, 2017) (**Figure 5A**). However, stable pheromone gradients may be rare in the wild, where cells mate in the context of tetrads (Taxis et al., 2005) (**Figure 5B**) or microcolonies (McClure et al., 2018) (**Figure 5C**). Even when surrounded by several potential partners, cells choose only one (Jackson and Hartwell, 1990a; Jackson and Hartwell, 1990b). It is unclear how such mating geometries could produce stable pheromone gradients yielding orientation toward just one partner (Jin et al., 2011; Rappaport and Barkai, 2012).

For successful mating, the pheromone landscape must be decoded to orient polarity toward the partner. However, imaging of polarity factors revealed that initial polarity sites were not always oriented toward the eventual mating partner (Henderson et al., 2019; Wang et al., 2019) or up-gradient in artificial pheromone gradients (Dyer et al., 2013; Hegemann et al., 2015; Jin et al., 2011; Kelley et al., 2015; Vasen et al., 2020a).

Rather, the location of the polarity site changed over time, stabilizing at better-oriented locations. In mating mixes, weak clusters of polarity factors appeared, disappeared, and

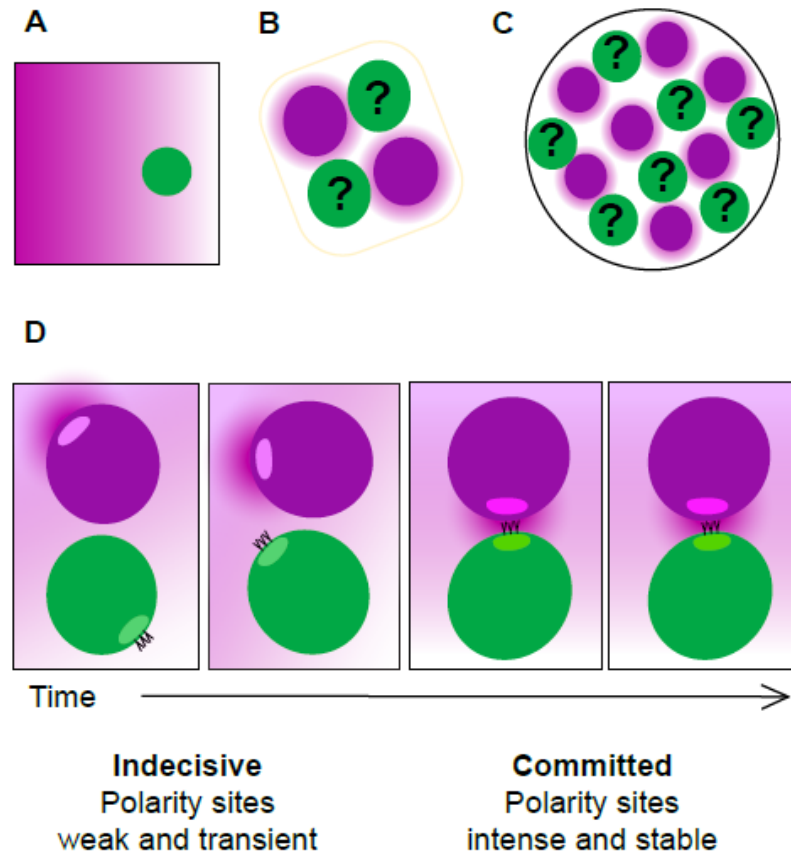


Figure 5: Pheromone landscapes encountered by yeast cells. (A) Stable unidirectional pheromone gradient, as generated by micropipet or microfluidics device. (B) Germinating spores in an ascus, where two potential partners (magenta) are expected to generate similar α -factor gradients, making them equally attractive to the a-cells (green). (C) Microcolony containing a mixture of a-(green) and α -cells (magenta). The proximity of multiple potential partners complicates the task of orienting toward a single partner. (D) Exploratory polarization model of partner selection. During the indecisive period (frames 1 and 2), diffusion of pheromone released at the α -cell's (magenta) polarity site yields a low pheromone concentration at the a-cell's (green) polarity site. When the two polarity sites are apposed, the a-cell senses a high concentration of pheromone. Both cells sense and secrete pheromone, but for simplicity, only the a-cell's receptors and α -cell's pheromone are shown.

changed position in a chaotic manner (Henderson et al., 2019). After this “indecisive phase” of 10-120 min, cells developed strong, stable polarity sites oriented toward the partner, suggesting that they made a “commitment” to the partner. Similarly, cells exposed to a steep pheromone gradient in a microfluidics device spent a variable interval with weak and mobile polarity sites before developing a strong polarity site at a stable position (Hegemann et al., 2015). These studies suggested that yeast cells process spatial information about the local pheromone landscape during a search period of variable duration, then commit to a specific orientation for polarized growth.

Spatial information about the pheromone landscape could be extracted by “global” or “local” sensing strategies (Hegemann and Peter, 2017; Kelley et al., 2015; Martin, 2019). In global sensing, cells compare the concentration of ligand-bound receptors around the cell surface to infer the direction of the pheromone source. In local sensing, cells primarily detect pheromone in a sensitized zone centered around the polarity site, moving the site around to infer the direction of the pheromone source. These models are not mutually exclusive.

Evidence for global sensing came from the observation that in mating mixes, initial weak polarity sites were oriented toward their eventual mating partners more often than would be expected by chance (Henderson et al., 2019). Thus, some spatial information was available before any polarity sites were visible. In principle, continued

global sensing during the indecisive phase (when polarity sites are weak and mobile) could promote the selection of optimal locations for stable “committed” polarity sites.

Evidence for local sensing came from the observation that when a strong polarity site is present, pheromone receptors and associated G proteins accumulate around the polarity site (Ayscough and Drubin, 1998; McClure et al., 2015; Suchkov et al., 2010). Thus, cells with a strong polarity site sense pheromone preferentially in the vicinity of the site. It is unclear whether the weak and transient polarity sites characteristic of the indecisive phase would similarly enable local sensing.

In *Schizosaccharomyces pombe*, weak and transient polarity sites in mating cells are enriched for pheromone secretion factors, as well as pheromone sensing factors (Merlini et al., 2016). If such enrichment is functionally important, then mobile polarity sites might represent the predominant sites of pheromone emission. These and other observations suggested a potential strategy for partner search that we call “exploratory polarization” (Henderson et al., 2019) (**Figure 5D**).

If cells secrete pheromone primarily from the indecisive polarity sites, then the pheromone landscape would change as the polarity sites move. If cells also sense pheromone primarily at the indecisive polarity sites, then the pheromone concentration they detect would depend on the distance to the nearest partner’s polarity site. When polarity sites are not properly aligned, the pheromone released from one site is dissipated by diffusion before it is detected at the partner’s polarity site (**Figure 5D**).

However, when two polarity sites face each other (and *only* in that case), a high concentration of pheromone is detected at each site (**Figure 5D**). In both *S. cerevisiae* and *S. pombe*, detection of a high pheromone concentration stabilizes the location of the polarity site (Bendezu and Martin, 2013; Dyer et al., 2013; McClure et al., 2015; Merlini et al., 2016). Thus, coincident detection of high pheromone levels upon alignment of partner polarity sites could stabilize both sites, leading to coordinated commitment by both partners.

Although the exploratory polarization hypothesis suggests an appealing strategy for partner selection, it is unclear to what degree pheromone secretion actually becomes polarized during the indecisive phase. If most pheromone is emitted globally from the entire cell surface, then that would create a stable pheromone gradient that could be decoded via either global sensing (Henderson et al., 2019) or local sensing (Hegemann 2015; Wang 2019). In this study, we show that as in *S. pombe*, transient polarity sites in *S. cerevisiae* are often enriched in pheromone sensing, signaling, and secretion proteins. Computational simulations provide quantitative support for the idea that pheromone levels sufficient to promote commitment are probably only achieved when polarity sites of mating partners become aligned. Most critically, we show that wildtype cells are unable to commit to partners that are impaired in the formation, localization, or stabilization of indecisive phase polarity sites. We conclude that local sensing and secretion by two cooriented polarity sites enables commitment by a mating pair.

2.2 Results

2.2.1 Pheromone sensing and secretion are enriched at transient polarity sites

Pheromone receptors and G proteins are concentrated near stable polarity sites (Ayscough and Drubin, 1998; McClure et al., 2015; Suchkov et al., 2010), but it was unclear whether the transient polarity sites characteristic of the indecisive period would similarly concentrate these factors. We imaged strains harboring both *BEM1-tdTomato* to label the polarity site and either *STE2-sfGFP* (receptor) or *GFP-STE4* ($G\beta$). In mating mixes, we identified time points at which Bem1 sites were clearly identifiable (**Figure 6A**) and assessed by visual comparison whether the Ste2 or Ste4 signal was colocalized with Bem1 (**Figure 6B**). Both the receptor and $G\beta$ were sometimes, though not always, colocalized with polarity factors (**Figure 6C**, **Figure 7A**).

We also examined pheromone secretion factors. The two pheromones are secreted by different mechanisms: α -factor is delivered to the plasma membrane in secretory vesicles, and a-factor is secreted by a transporter, Ste6 (Michaelis and Barrowman, 2012). As with the pheromone sensing probes, GFP-Sec4 (a marker of secretory vesicles) and Ste6-sfGFP were often enriched at indecisive polarity sites (**Figure 6B**, **Figure 7A**). Because colocalization can occur while Bem1-containing polarity sites are still mobile, these data suggest that even transient polarity sites can create detectable enrichment of pheromone sensing and secretion proteins.

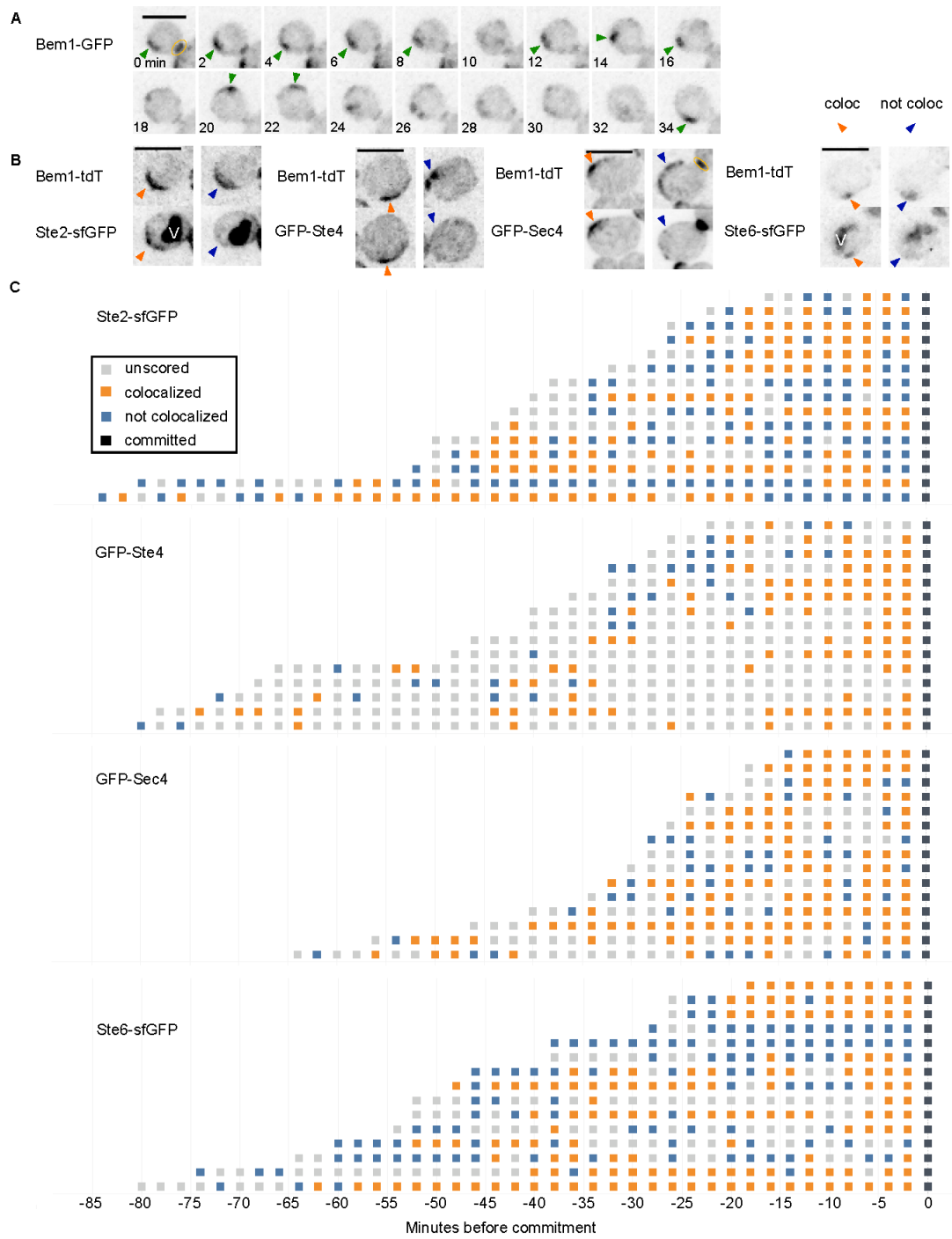


Figure 6: Localization of pheromone secretion, sensing, and signaling proteins during the indecisive period. (A) Example cell showing Bem1 (polarity marker) behavior during the indecisive phase. Strains harboring Bem1-tdTomato (DLY12943) were mixed with wildtype (DLY9070) and imaged. Scale bar: 4 μ m. For scoring colocalization, Bem1 distributions were considered either scorable (1 or 2 predominant Bem1 clusters or a Bem1 crescent, green arrowheads) or not scorable (diffuse, weak, and/or multiple Bem1 clusters, no arrowhead). See Figure S1. (B) Example images from scorable time points during the indecisive phase, in which the indicated probes were scored as colocalized (orange arrowhead) or not colocalized (blue arrowhead) with Bem1. Strains harboring Bem1-tdTomato and either the α -factor receptor Ste2-sfGFP (DLY22243), G β subunit GFP-Ste4 (DLY23354), secretory vesicle marker GFP-Sec4 (DLY13771), or a-factor transporter Ste6-sfGFP (DLY22355) were mixed with wildtype (DLY8156) and imaged. Internal signal in Ste2-sfGFP and Ste6-sfGFP strains is due to sfGFP accumulation in the vacuole (V) following Ste2/Ste6 degradation. Yellow oval: cytokinesis site. Scale bars: 5 μ m. (C) Cell behaviors during the indecisive phase, scored from the same mating mixes as in (B). Cells that experienced an indecisive period of >5 time points were tracked either from the beginning of the movie (if already in G1) or from birth (appearance of Bem1 at the neck) until commitment. Each row represents one cell: each timepoint was designated as not scorable (grey box) or scorable, and the latter were scored as colocalized (orange box) or not colocalized (blue box). x-axis: minutes before commitment.

Indecisive polarity site behavior was also seen in cells treated with a low but uniform level of α -factor (**Figure 7B**), suggesting that such behavior reflects the overall pheromone sensed by the cell and does not require a pheromone gradient. Nevertheless, the frequent orientation of polarity sites toward potential partners during the indecisive stage (Henderson et al., 2019) suggests that polarity location is influenced by pheromone gradients at this stage.

2.2.2 Simulating the pheromone landscape experienced by mating cells

Our findings support the possibility that pheromone is emitted locally from the polarity site. To understand how local, as opposed to global, pheromone emission

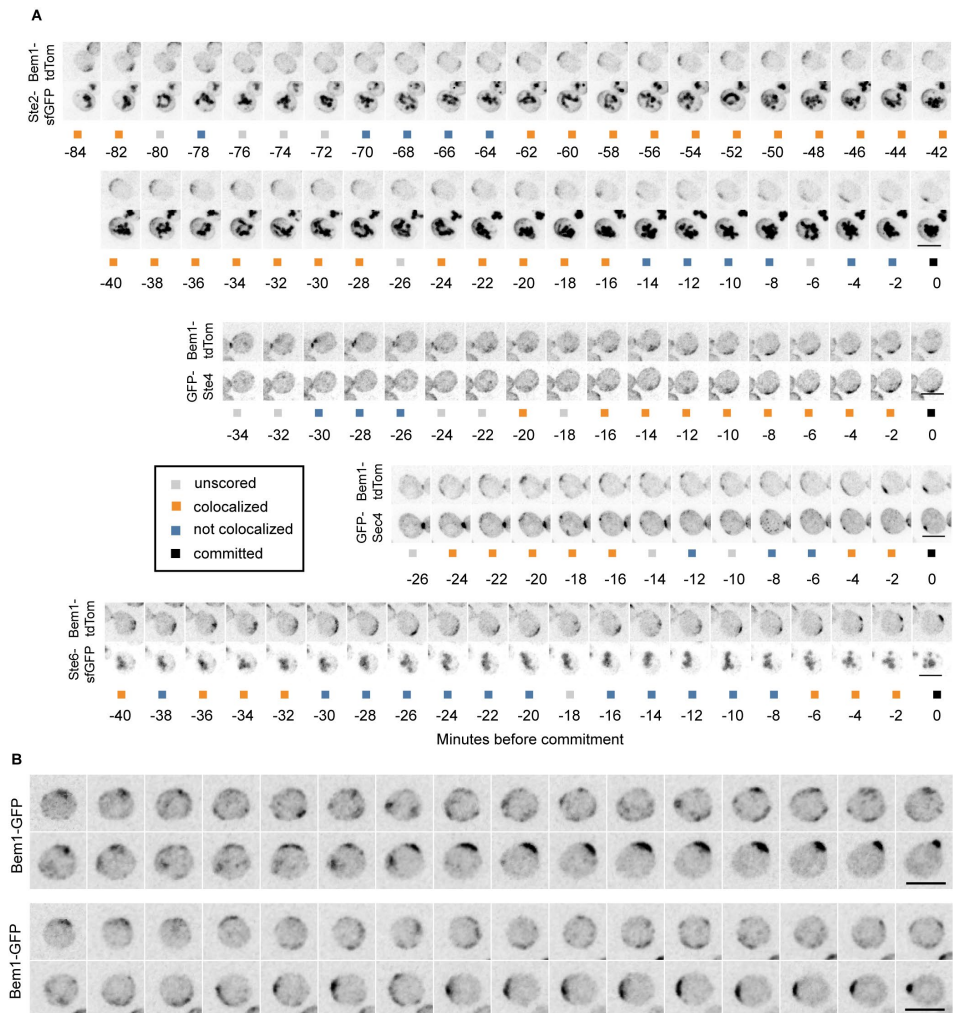


Figure 7: Cell behavior during the indecisive period. (A) Example montages showing time courses during the indecisive period, along with assigned colocalization score. Strains harboring Bem1-tdTomato and either the α -factor receptor Ste2-sfGFP (DLY22243), G β subunit GFP-Ste4 (DLY23354), secretory vesicle marker GFP-Sec4 (DLY13771), or a-factor transporter Ste6-sfGFP (DLY22355) were mixed with wildtype (DLY8156) and imaged. Internal signal in Ste2-sfGFP and Ste6-sfGFP strains is due to sfGFP accumulation in the vacuole following Ste2/Ste6 degradation. Colocalization scores for individual time points are indicated by colored squares. There is an unavoidable level of subjectivity in applying this scoring procedure. (B) Two a cells (DLY23016) treated with 5 nM α -factor show indecisive behavior during G1, then polarize and bud. Cells lack the α -factor-degrading Bar1 protease to ensure a stable pheromone concentration throughout the imaging period. Interval between frames: 2 min. Scale bars: 5 μ m.

would affect the pheromone landscape sensed by the partner, we first used solutions of the diffusion equation to estimate the pheromone concentration that is expected to be detected next to a cell secreting pheromone. An α cell exposed to **a**-factor secretes approximately 1400 molecules of α -factor per second (Rogers et al., 2012). Assuming that the pheromone profile reaches steady state, a cell that secretes pheromone globally would generate a local pheromone concentration at the surface of a neighboring cell of only 0.5 nM (Materials and Methods). However, if pheromone were secreted in a focused manner, the local concentration could exceed 5 nM, comparable to the receptor K_D (Jenness and Spatrack, 1986).

To better understand how a “local sensing” cell that detects pheromone at a zone surrounding the polarity site would respond to an adjacent partner, we simulated an arrangement with two spheres: a pheromone emitter and a pheromone receiver. The spheres were 250 nm apart (the minimal possible distance based on the combined thickness of two cell walls) to simulate cells that are touching (**Figure 8A**). α -factor is secreted by exocytosis of vesicles, which fuse at a rate of $\sim 0.83/s$ (Dyer et al., 2013). Thus, with an overall α -factor release rate of 1400/s (Rogers et al., 2012), the average number of pheromone molecules in a vesicle would be ~ 1680 .

We simulated pheromone release in one of two patterns: global secretion, where each vesicle releases its pheromone at a random position on the surface of the emitter, or

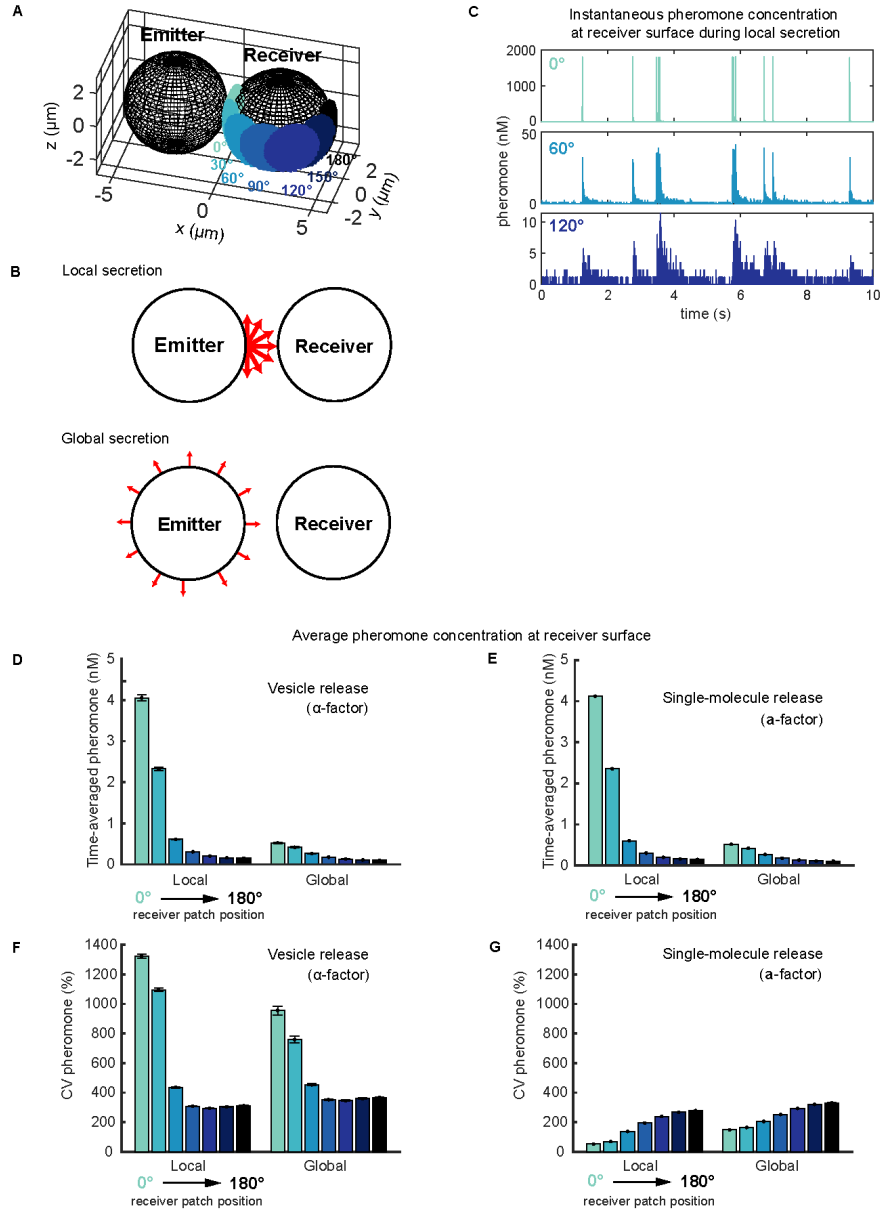


Figure 8: Simulations of the pheromone receiver's landscape for two touching cells. (A) Model setup for emitter and receiver cells shown at scale. Seven patch positions on the receiver (0° to 180°, changing colors) were used to measure local pheromone concentrations. (B) Local versus global secretion. In local secretion, pheromone was released at the emitter pole abutting the receiver. In global secretion, pheromone was released uniformly at the emitter surface. (C) Instantaneous pheromone concentration at different positions (color) near receiver's surface over time during local vesicle secretion. (D,E) Time-averaged pheromone concentration at different positions (color) on receiver's surface for both vesicle and single-molecule release. (F,G) Coefficient of variation (CV) for (D,E). All bars show mean \pm s.e.m., n = 300 realizations.

local secretion, where each vesicle releases pheromone at the pole that abuts the receiver (**Figure 8B**). Following secretion, pheromone molecules were assumed to diffuse freely unless reflected from the surfaces of the two spheres. To simulate pheromone sensing in the vicinity of the polarity site, we designated a $\sim 1.3 \mu\text{m}$ diameter patch at several locations (0° to 180°, changing colors, **Figure 8A**) on the receiver, and counted the number of molecules within $0.25 \mu\text{m}$ of the patch surface. Pheromone concentrations calculated in this manner fluctuated dramatically as vesicles were released (**Figure 8C** and **Figure 9**).

Pheromone-receptor binding and unbinding are slow ($k_{\text{off}} = 0.01\text{-}0.001/\text{s}$) (Bajaj et al., 2004; Jenness et al., 1983; Raths et al., 1988; Yi et al., 2003), and, therefore, receptors are unable to respond rapidly to transient spikes in pheromone concentration. This suggests that receptors would time average the local concentration. Temporal averaging of simulated pheromone concentrations in different patches on the receiver cell indicated that the concentration sensed in the patch facing the emitter was ~ 8 -fold

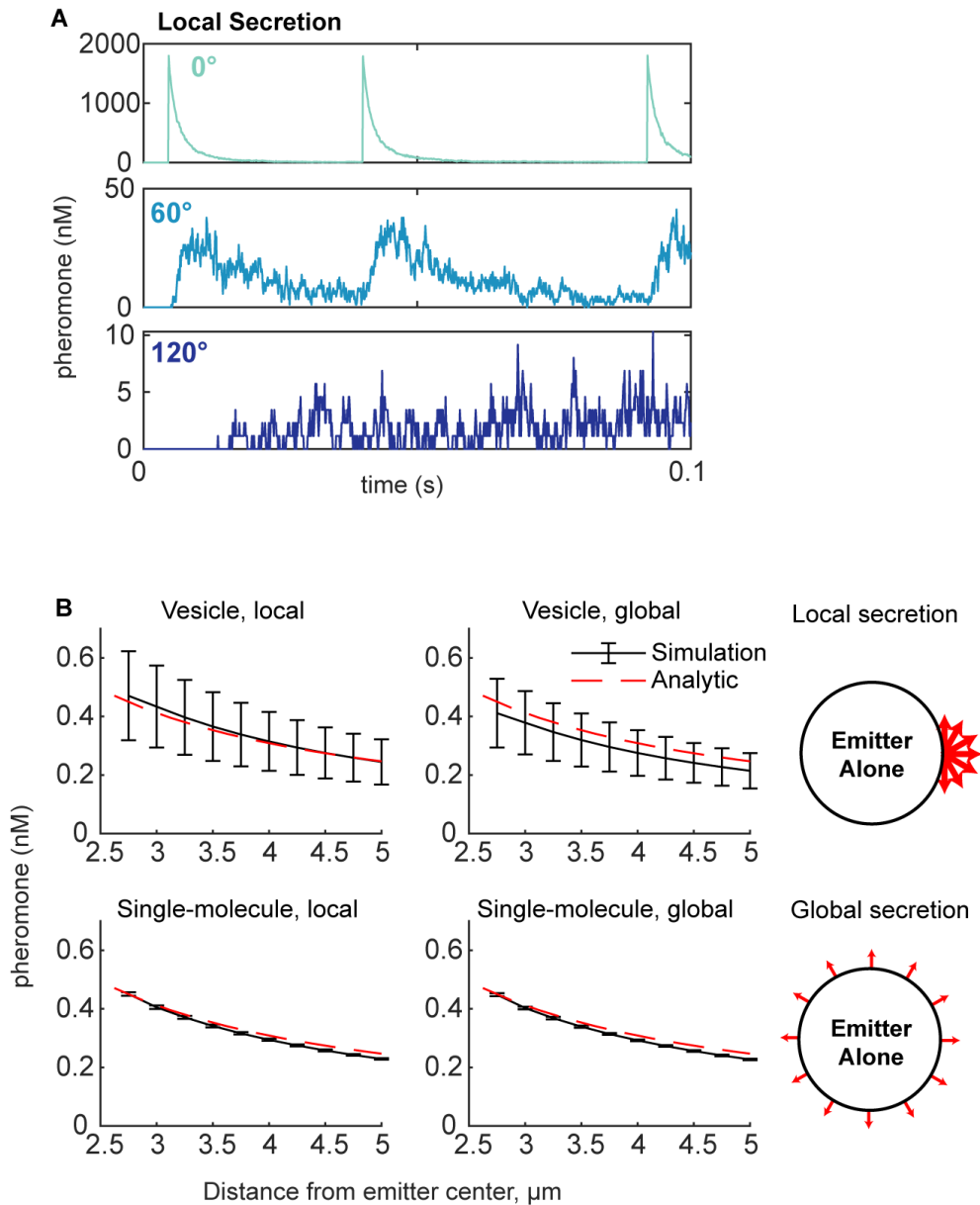


Figure 9: Validation of the pheromone simulations and additional detail. (A) Pheromone concentrations perceived at three different patches in a single simulation as in Figure 3C, but zoomed in to show 0.1 second along the x-axis. (B) Simulations of the emitter alone, comparing concentrations in a spherical 250 nm shell (not a patch) at the indicated distance from the center of the emitter versus the steady-state analytic solution of the diffusion equation under equivalent conditions. Bars show mean \pm s.d., $n = 30$.

higher for simulations with polarized secretion compared to those with global secretion, consistent with the estimates discussed above (**Figure 8D**). Thus, if a threshold concentration must be detected to promote commitment, then cells that secrete pheromone in a polarized manner would be much more likely to cross that threshold. Furthermore, the pheromone concentrations sensed at different locations declined much more rapidly with distance from the emitter in the simulations with polarized secretion (**Figure 8D**). The steeper gradients created by polarized secretion may also be important for locating a mating partner. Thus, when secretion and sensing both occur at polarity sites, the concentration sensed by a cell would depend on the relative positions of the two cells' polarity sites, as posited by the exploratory polarization hypothesis.

Unlike α -factor, **a**-factor is exported by the transporter Ste6 (Michaelis and Barrowman, 2012), so that **a**-factor release may occur one molecule at a time (Michaelis and Barrowman, 2012), rather than in vesicular packets. We repeated the simulations assuming the same overall production rate but releasing one molecule of pheromone at a time. While the variability in pheromone concentration was greatly reduced (**Figure 8G**, compare with **F**), the average pheromone concentrations sensed at different locations remained the same (**Figure 8E**, compare with **D**). In summary, local pheromone secretion would lead to ~8-fold higher pheromone levels at the interface between partners.

2.2.3 Wildtype cells fail to commit to constitutively indecisive partners

Our findings indicate that pheromone secretion might be polarized during the indecisive phase, and that if it is, that would significantly alter local pheromone levels. But is polarized secretion important for communication to a partner cell? If pheromone emission is mainly global, then partner cells would commit to a partner regardless of that partner's polarity site behavior. On the other hand, if pheromone emission is mainly local, the behavior of the polarity sites would be critical, and a cell would only commit to a partner that was reciprocating by stabilizing its own polarity site. To distinguish between these models, we explored the behavior of wild-type cells exposed to mutant partners that display constitutively indecisive polarity sites.

To quantify polarity site behavior, we developed an unbiased "spatial autocorrelation" scoring method to distinguish indecisive and committed polarity sites based on the Bem1 probe (**Figure 10A**). We calculated the correlation between the spatial distribution of pixel intensities in a cell in consecutive time points. When polarity sites are mobile, the correlation is low, but if the cells commit, the correlation is high. We selected an autocorrelation threshold to designate commitment (**Figure 10B**). In wildtype mating mixes where cells committed and fused with partners (**Figure 11A, 12A**), 19/20 α cells and 48/50 α cells crossed the threshold (**Figure 11C,E, 10C,D**).

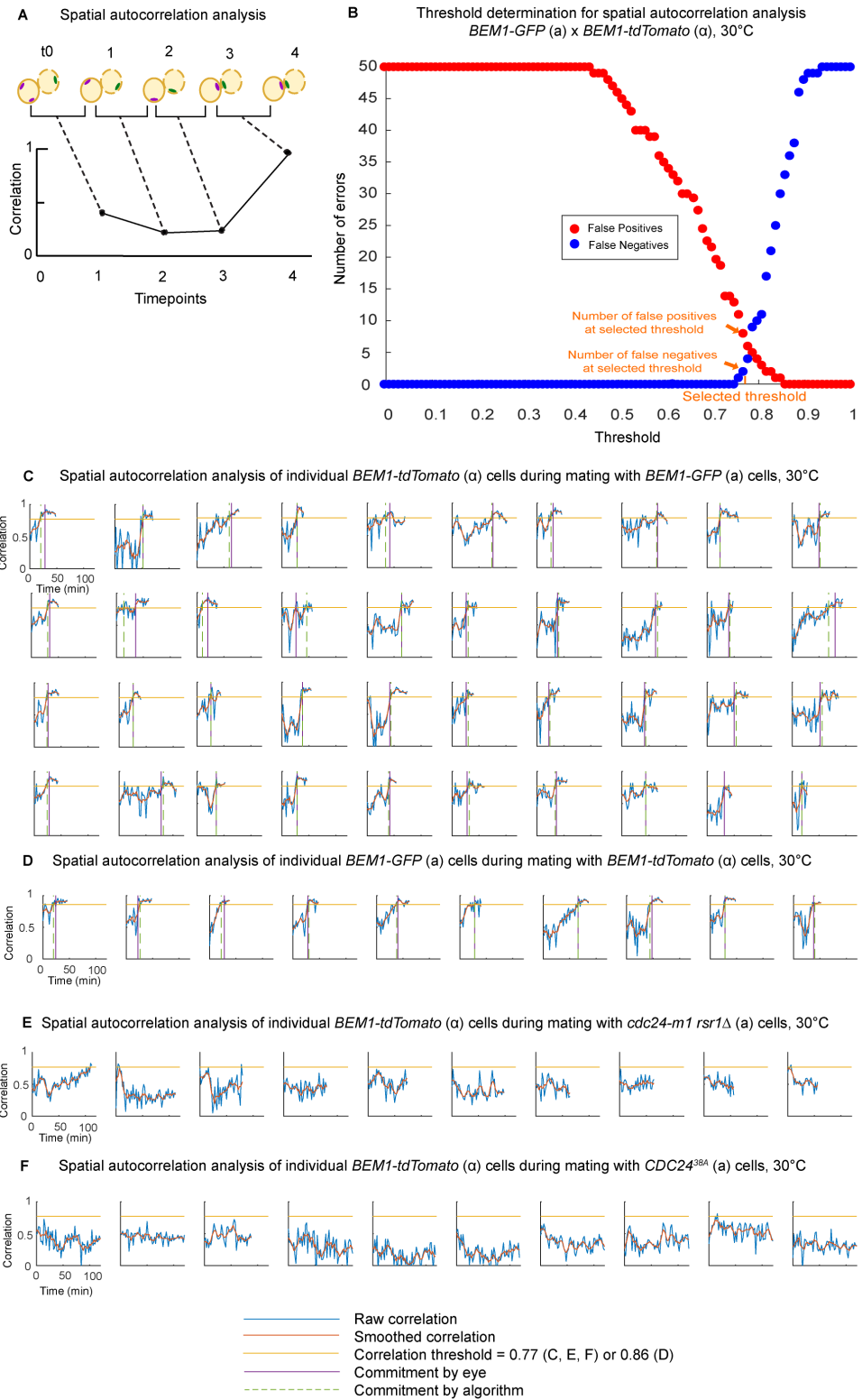


Figure 10: Spatial autocorrelation metric. (A) Cartoon illustrating spatial autocorrelation algorithm to score commitment. The spatial distribution of Bem1 pixel intensities in a cell of interest (magenta clusters) are compared at consecutive time points to yield a normalized correlation measure between 0 (no correlation) and 1 (perfect correlation). Strong and stably oriented polarity sites characteristic of committed cells (3,4) yield a high correlation while weaker, mobile polarity sites characteristic of indecisive cells (0,1,2) yield a low correlation. (B) Threshold determination for scoring commitment. The number of false negatives (in which the spatial autocorrelation trace did not cross the threshold but did commit as scored visually) and false positives (in which the spatial autocorrelation trace crossed the threshold > 4 min before commitment as scored visually) as a function of commitment threshold. A threshold of 0.77 was selected (orange tick). (C,D) Spatial autocorrelation traces for 40 additional wildtype α -cells (C) and 10 additional a-cells (D) from wildtype by wildtype mixes at 30°C, from the time of the cell's entry into G1 to the time point preceding fusion. (E,F) Spatial autocorrelation traces for 10 wildtype cells mixed with *cdc24-m1 rsr1 Δ* (E) or *CDC24^{38A}* (F) cells, from the time of the cell's entry into G1 to the end of the movie. x-axis: Time (min). y-axis: spatial autocorrelation (yellow line: commitment threshold). Commitment to a partner as determined visually (vertical purple line) or by crossing the threshold (dashed green line).

Polarity site stabilization (commitment) occurs by two parallel pathways, each of which recruits the Cdc42-directed guanine nucleotide exchange factor (GEF) Cdc24 to the cortex (Dyer et al., 2013). One pathway depends on binding of the scaffold Far1 to Cdc24, which is impaired in the *cdc24-m1* mutant (Butty et al., 1998; Nern and Arkowitz, 1998; Nern and Arkowitz, 1999; Valtz et al., 1995). The other depends on the Ras-family GTPase Rsr1 (Bender and Pringle, 1989; Chant and Herskowitz, 1991). When treated with concentrated pheromone, mutants lacking both of these pathways (*cdc24-m1 rsr1 Δ*) exhibit constitutively mobile polarity sites (Dyer et al., 2013; Nern and Arkowitz, 2000), and we found that they also exhibited constitutively mobile sites in a mating mix, with spatial autocorrelation remaining low (Figure 11B,D, 12B). Consistent with earlier work

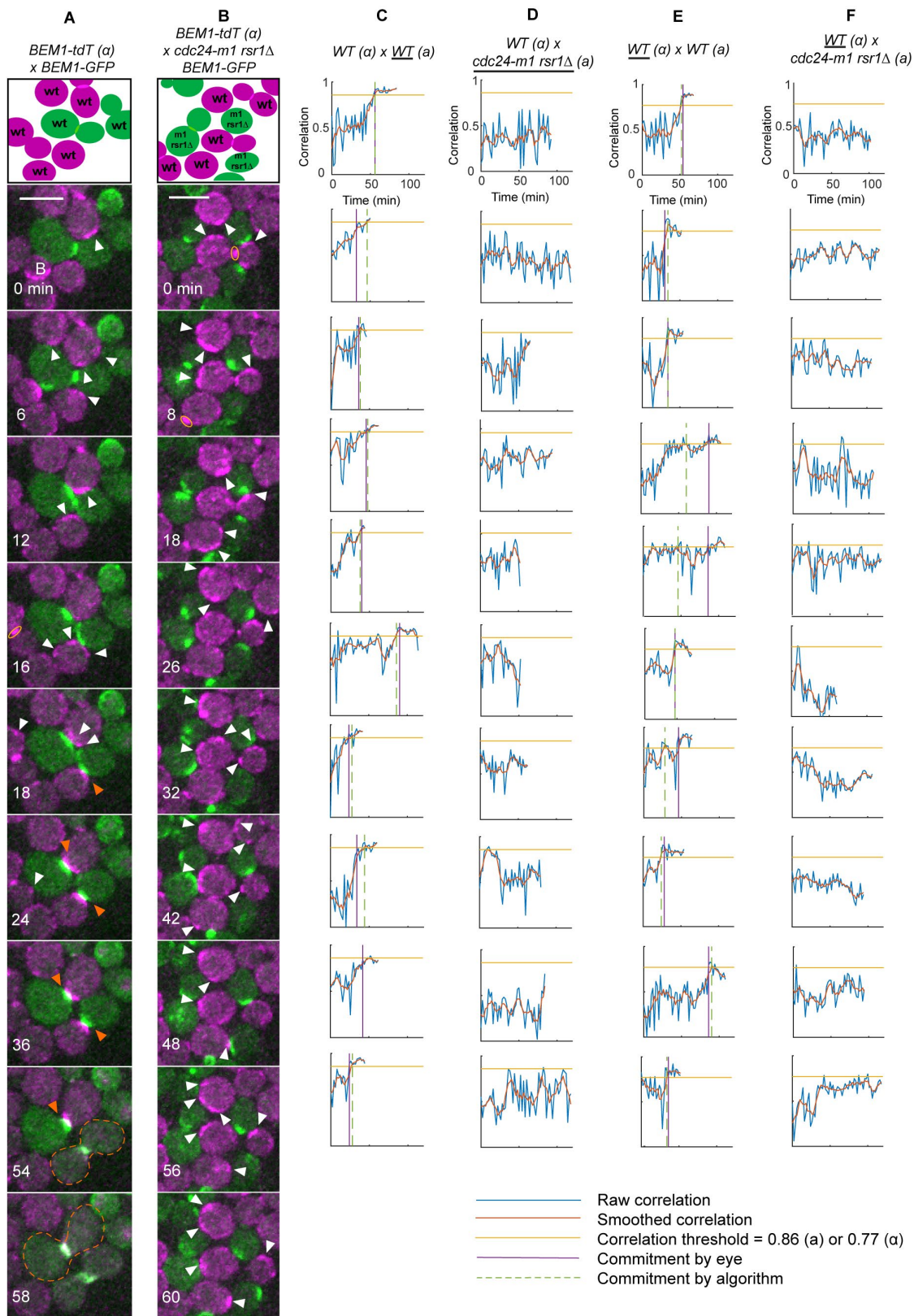


Figure 11: Wildtype cells do not commit to mutants with constitutively mobile polarity sites. (A,B) Selected time points from movies of mating mixes imaged at 30°C. Cartoons indicate cells in the selected montages at the start of the displayed imaging interval. Yellow oval: mother-bud neck. White arrowhead: weak mobile Bem1-tdTomato clusters in wildtype partners. Orange arrowheads: stably oriented Bem1 clusters characteristic of committed cells. Dashed outline: fused zygote. (A) MAT α wildtype cells (DLY12944, magenta) mixed with MATa wildtype cells (DLY9069, green). (B) MAT α wildtype cells (DLY12944, magenta) mixed with MATa mutants that form constitutively mobile polarity clusters (*cdc24-m1 rsr1 Δ* , DLY22797, green). (C,D) Spatial autocorrelation traces of representative wildtype (C) or *cdc24-m1 rsr1 Δ* (D) cells mixed with wildtype α partners. Traces represent cells with the underlined genotype (a). (E,F) Spatial autocorrelation traces of representative wildtype α cells mixed with wildtype (E) or *cdc24-m1 rsr1 Δ* (F) partners. Horizontal yellow line: threshold autocorrelation used to call commitment. Purple vertical line: commitment time as scored visually. Wildtype cells attempting to mate with constitutively indecisive mutants did not reach the threshold.

(Nern and Arkowitz, 1999), mating mixes between wildtype and *cdc24-m1 rsr1 Δ* strains showed very poor mating efficiency (1/274 cells mated in mutant mix, n = 2 movies, but 305/503 cell mated in wildtype mix, n = 4 movies).

In control mating mixes with wildtype **a** cells, wildtype α cells committed to a partner after a variable indecisive phase (magenta cells in **Figure 11A**). However, when mixed with *cdc24-m1 rsr1 Δ* **a** cells, wildtype α cells failed to commit, instead exhibiting prolonged indecisive behavior (magenta cells in **Figure 11B**). Similar results were obtained when wildtype **a** cells were mixed with *cdc24-m1 rsr1 Δ* α cells (**Figure 12**). Unlike in wildtype mating mixes, in mating mixes with *cdc24-m1 rsr1 Δ* partners 0/20 wildtype cells (α) crossed the spatial autocorrelation threshold (**Figure 11F, 10E**). We conclude that wildtype cells cannot commit to a constitutively indecisive partner.

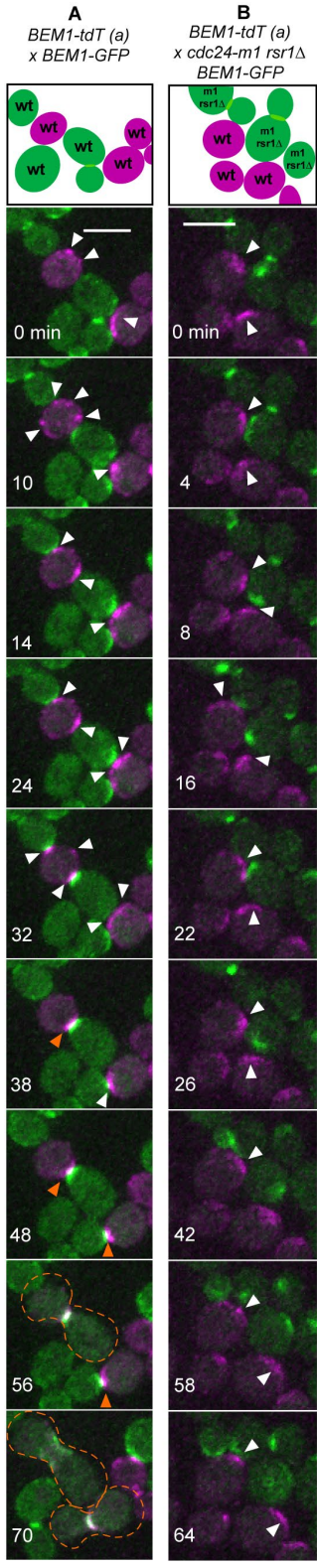


Figure 12: Wildtype cells do not commit to partners with constitutively mobile polarity sites, regardless of mating type. Selected time points from movies of mating mixes. White arrowhead: weak mobile Bem1 cluster characteristic of indecisive cells, focusing on the magenta wildtype cells. Orange arrowheads: stably oriented Bem1 clusters characteristic of committed cells. Dashed outline: fused zygote. (A) MAT α wildtype cells (DLY12943, magenta) were mixed with MAT α wildtype cells (DLY9070, green). Mating type and fluorophore are switched relative to Figure 11A. (B) MAT α wildtype cells (DLY12943, magenta) were mixed with MAT α mutants that form constitutively mobile polarity clusters (*cdc24-m1 rsr1 Δ* , DLY23612, green). Mating type switched relative to Figure 11B. Scale bars: 5 μ m.

A potential caveat to our conclusion was that the failure of wildtype cells to commit to *cdc24-m1 rsr1 Δ* mutants might be due to the mutants secreting less pheromone than wildtype cells. To measure pheromone secretion, we used the halo assay, in which cells from one mating type are deposited onto a spot over a lawn of cells of the opposite mating type. As the cells in the broader lawn proliferate, the pheromone released from the spotted cells causes cell-cycle arrest of nearby cells in the lawn, creating a “halo” (no-growth zone) whose diameter reflects the amount of pheromone released (see Methods) (Manney, 1983). Halo assays indicated that *cdc24-m1 rsr1 Δ* cells secreted comparable levels of pheromone to wildtype cells (both a-factor and α -factor) (Figure 13). These findings suggest that commitment by one partner requires reciprocal commitment by the other, consistent with the exploratory polarization hypothesis.

2.2.4 Behavior of wildtype cells mixed with prematurely committed partners

If wildtype cells cannot commit to partners that are constitutively indecisive, what about partners that commit prematurely? Addition of saturating levels of α -factor

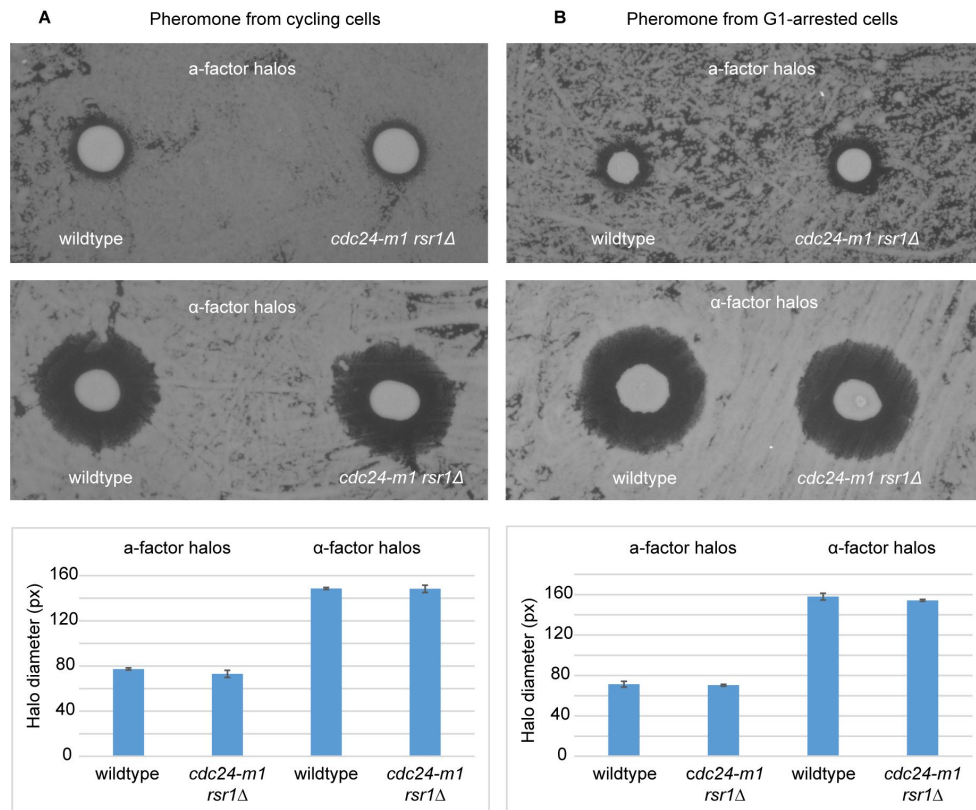


Figure 13: Wildtype and *cdc24-m1 rsr1Δ* mutants secrete similar amounts of pheromones. Halo assays were conducted as described in Methods. (A) Spots of MAT_a wildtype (DLY9069) and *cdc24-m1 rsr1Δ* (DLY22797) generate similar a-factor halos, and spots of MAT_α wildtype (DLY9070) and *cdc24-m1 rsr1Δ* (DLY23612) generate similar α-factor halos. (B) Spots of MAT_a wildtype (DLY20628) and *cdc24-m1 rsr1Δ* (DLY22532) cells arrested in G1 by expression of Ste5-CTM generate similar a-factor halos, and spots of MAT_α wildtype (DLY20625) and *cdc24-m1 rsr1Δ* (DLY22533) arrested in G1 by expression of Ste5-CTM generate similar α-factor halos.

Quantification: mean +/- SEM halo diameter for n = 3 plates.

to a mating mix causes the a partner to polarize stably. As α-factor is everywhere, the a cell is “confused”, and polarizes in a random direction relative to the partner, resulting in a significant reduction of mating efficiency (Dorer et al., 1997; Dorer et al., 1995). It is not known whether successful mating events in these conditions reflects a “unilateral”

mating in which only one partner needs to orient properly, or a fortuitous coorientation between a “confused” **a** cell and an α partner.

We imaged wildtype cells in a mating mix with 10 μ M α -factor. **a** cells polarized stably and grew in a single direction which usually did not point to an α partner. The α cells next to such “misoriented” **a** cells exhibited prolonged indecisive behavior and did not commit or mate (**Figure 14A**). In the rarer instances in which an **a** cell polarized toward an α partner, some α cells polarized toward the **a** cell’s polarity site and mated (**Figure 14B**). Thus, cells can mate with partners that stably orient in the correct direction, even if that orientation develops by chance and not through a search process. This accounts for all of the mating events we observed (n = 14). Interestingly, we also observed instances where pairs that appeared to be properly cooriented failed to mate (n = 36) (**Figure 14C**). The basis for this behavior remains unknown. Curiously, cells were able to mate even if the polarity site of the α partner was less stable than in typical pairings, as reflected in the fact that the spatial autocorrelation metric did not reach the commitment threshold (**Figure 14D**). Cells that did not mate (regardless of orientation) never reached the commitment threshold (**Figure 14D**). We did not observe any fusion events without preceding coorientation, suggesting that only if the two partners’ polarity sites are oriented toward each other do the cells commit and mate.

Figure 14: Mating in “pheromone confusion” conditions. (A-C) Selected time points from movies of wildtype by wildtype mating mixes in the presence of 10 μ M α -factor. MAT α cells (DLY12944, magenta) were mixed with MAT α cells (DLY9069, green, “confused” by excess pheromone). Confused cells polarize stably and form mating projections. White arrowhead: weak mobile Bem1 clusters in the MAT α partners (magenta). (A) When MAT α cell projections are oriented away from a potential partner, the partner’s polarity sites remain indecisive. (B) When MAT α cell projections are oriented towards a potential partner, the cells can mate. (C) Mating can fail despite apparently correct orientation by the confused partner. (D) Representative spatial autocorrelation traces of MAT α cells from instances of the categories illustrated in (A-C).

2.2.5 Wildtype cells fail to commit to partners that lack polarity sites

Our findings thus far suggest that pheromone is emitted locally at polarity sites even during the indecisive phase, and that local emission at cooriented polarity sites is required in order to trigger commitment. If that is the case, then a cell that secreted pheromone globally would be unable to trigger commitment in its partner. To test that prediction, we wished to ask how wildtype cells respond to partners that cannot polarize Cdc42.

We first considered cells unable to activate Cdc42. At the restrictive temperature, *cdc24-4^{ts}* mutants fail to polarize and have predominantly inactive Cdc42-GDP (Adams et al., 1990; Atkins et al., 2013). However, *cdc24-4^{ts}* mutants also fail to activate the Cdc42 effector kinase Ste20 and cannot respond to pheromone (Simon et al., 1995; Zhao et al., 1995), so we introduced the constitutive *ste20^{ACRIB}* in an attempt to restore pheromone signaling (Moskow et al., 2000). At restrictive temperature, wildtype cells failed to commit to unpolarized *cdc24-4^{ts} ste20^{ACRIB}* mutants (**Figure 15**), consistent with the

A *BEM1-GFP (α)*
x *cdc24-4^{ts} BEM1-tdT*

B *BEM1-GFP (α)*
x *cdc24-4^{ts} BEM1-tdT*

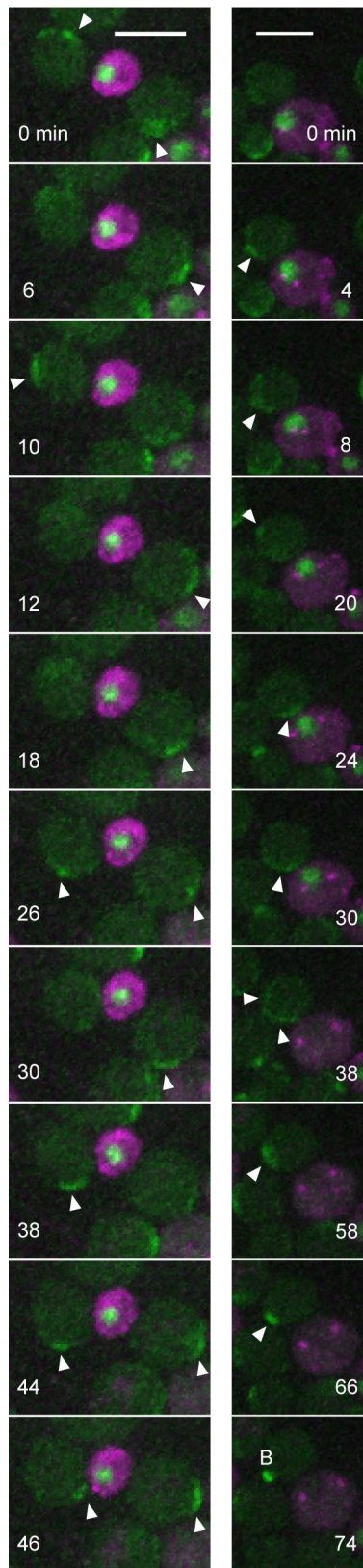


Figure 15: Behavior of *cdc24-4^{ts} ste20^{ΔCRIB}* mutants in mating mixes. Time-lapse movies of mating mixes with wild-type (DLY9070, green) and mutant (DLY23256, magenta with green nuclei) partners grown at 30°C or 24°C, respectively, and shifted to a pre-warmed agarose slab for imaging at 37°C. (A) Montage showing mutant daughter cell that remains arrested in G1 and wildtype partner that remains indecisive. (B) Montage showing mutant mother that exits G1 (Whi5 leaves nucleus at 38 min). While many small mutant daughter cells remained arrested, the larger mothers did not. In all cases, the wildtype partners failed to commit. B: bud. Scale bars: 5 μm.

hypothesis that global pheromone emission is not sufficient to trigger commitment.

However, interpretation of this result was complicated by the observation that *cdc24-4^{ts} ste20^{ΔCRIB}* mutants often failed to maintain G1 arrest (**Figure 15**). We were able to enforce G1 arrest of the mutants (mating type **a**) by adding 10 μM α-factor. Pre-treatment with α-factor at restrictive temperature caused the mutants to arrest as large unpolarized cells in G1 (see below). In mating mixes, wildtype α partners adjacent to these unpolarized mutants were efficiently arrested in G1 (91% of cells adjacent to a mutant remained unbudded for the median time of arrest in wildtype mixes, n = 142 cells, 3 movies). However, we did not observe mating between wildtype and mutant cells (0/83 cells mated to mutants, compared to 92/115 cells mated to wildtype partners at 35°C).

Wildtype cells committed to other wildtype cells (green cells in **Figure 16A**), but when mixed with unpolarized *cdc24-4^{ts} ste20^{ΔCRIB}* mutants, they failed to commit and exhibited prolonged indecisive behavior (green cells in **Figure 16B**). We could not use the same spatial autocorrelation threshold for analysis of cells at 35°C (**Figure 16B**) because polarity sites were less bright and more mobile at 35°C than 30°C. Based on

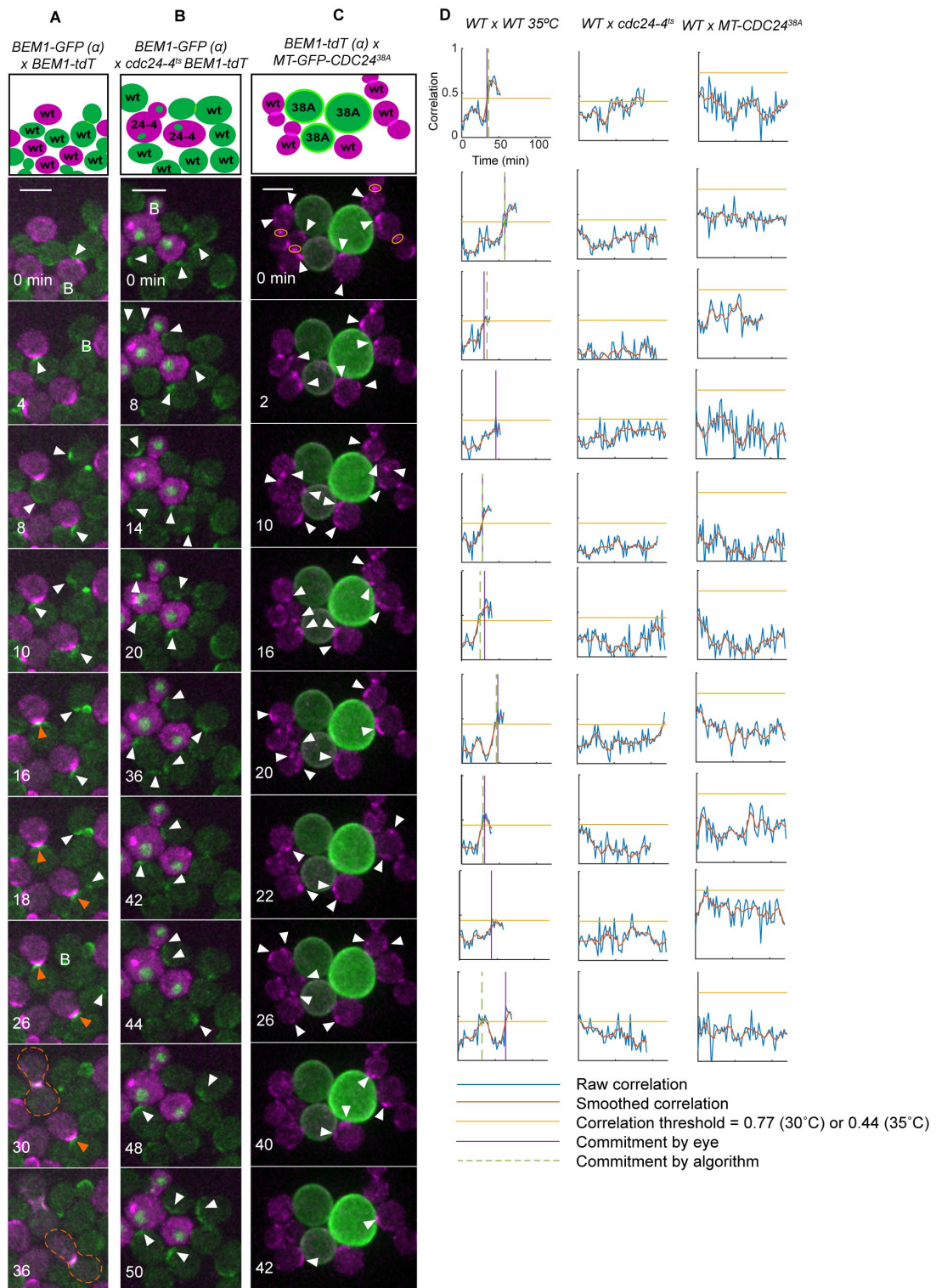


Figure 16: Wildtype cells do not commit to unpolarized partners. Selected time points from movies of mating mixes. B: bud. Yellow oval: mother-bud neck. White arrowhead: weak, mobile clusters in wildtype partners. Orange arrowheads: stably oriented Bem1 clusters characteristic of committed cells. Dashed outline: fused zygote. 10 μ M α -factor was added to (B) and (C) to sustain G1 arrest of mutant MATa cells. (A) MAT α wildtype cells (DLY9070, green) mixed with MATa wildtype cells (DLY12943, magenta), imaged at 37°C. (B) The same MAT α wildtype strain mixed with *cdc24-4^{ts} ste20 Δ ^{CRIB}* MATa cells (DLY23256, nuclear accumulation of Whi5-GFP, green, indicates G1 cells), imaged at 35°C. (C) MAT α wildtype cells (DLY12944, magenta) mixed with MATa cells harboring membrane-targeted, constitutively-active Cdc24 (MT-GFP-CDC24^{38A}, DLY23351) that do not make polarity clusters. Scale bars: 5 μ m. (D) Example spatial autocorrelation traces from wildtype cells mixed with the indicated partners. Horizontal yellow line: threshold autocorrelation used to call commitment. Purple vertical line: commitment time as scored visually. Wildtype cells attempting to mate with unpolarized mutants did not reach the threshold, even after 100 min.

wildtype mating mixes at 35°C, we chose a different threshold to score commitment (Figure S17A,B). Using that threshold, 42/50 wildtype cells committed in matings with wildtype partners, while only 5/20 wildtype cells committed in mating mixes with *cdc24-4^{ts} ste20 Δ ^{CRIB}* partners (Figure 16D, S17C). These findings suggest that wildtype cells cannot commit to a partner lacking GTP-Cdc42.

Because loss of Cdc42-GTP may have consequences beyond the absence of polarity sites, we also sought to eliminate polarity sites by activating Cdc42 all over the cortex. To that end, we overexpressed a membrane-targeted, constitutively-active Cdc24 (MT-GFP-CDC24^{38A}), a strategy previously shown to abrogate polarization (Kuo et al., 2014). Induction of membrane-targeted Cdc24^{38A} blocks budding but allows cell cycle progression until G2, where cells arrest due to the morphogenesis checkpoint (Lew, 2003). To ensure that the mutants (mating type a) were arrested in G1, we added 10 μ M

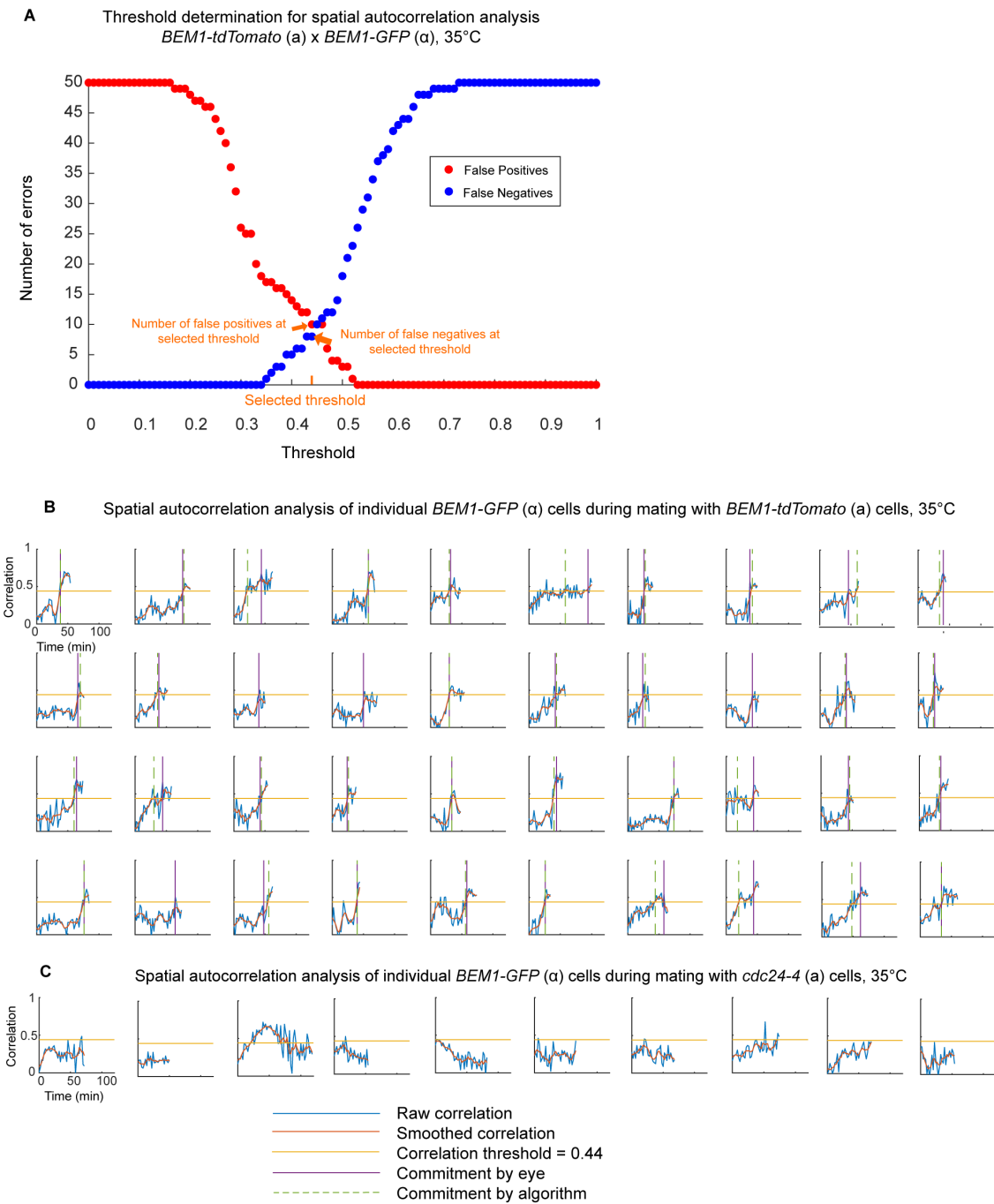


Figure 17: Threshold determination for spatial autocorrelation at 35°C. (A) Threshold determination for scoring commitment. The number of false negatives (in which the spatial autocorrelation trace did not cross the threshold but did commit as scored visually) and false positives (in which the spatial autocorrelation trace crossed

the threshold > 4 min before commitment as scored visually) as a function of commitment threshold. A threshold of 0.44 was selected (orange tick). (B) Spatial autocorrelation traces for 40 additional wildtype by wildtype pairs at 35°C, from the time of the cell's entry into G1 to the time point preceding fusion. (C) Spatial autocorrelation traces for 10 wildtype by *cdc24-4* pairs at 35°C, from the time of the cells' entry into G1 until the end of the movie. x-axis: Time (min). y-axis: spatial autocorrelation (yellow line: commitment threshold). Commitment to a partner as determined visually (vertical purple line) or by crossing the threshold (dashed green line).

α -factor. In arrested mutant cells, both Bem1-tdTomato and *MT-GFP-Cdc24^{38A}* were broadly distributed on the plasma membrane (**Figure 18**). In mating mixes, wildtype α partners adjacent to these unpolarized mutants arrested efficiently in G1 (94% of cells adjacent to a mutant remained unbudded for the median duration of arrest in wildtype mixes, n = 116 cells, 3 movies). However, wildtype and mutant cells did not mate, even when imaged for 3 h (0/151 cells mated to mutants, compared to 100/162 cells mated to wildtype partners).

When mixed with *MT-GFP-CDC24^{38A}* mutants, the wildtype α cells did not commit, instead displaying extended indecisive behavior (**Figure 15C**). Whereas 48/50 cells mixed with wildtype partners developed spatial autocorrelation above threshold, 0/20 cells mixed with *MT-CDC24^{38A}* partners did so, despite prolonged imaging (**Figure 15D, 12D**). We conclude that indecisive polarity sites are critical to communicate a cell's location to its partner, and that without such communication, a wildtype cell does not commit.

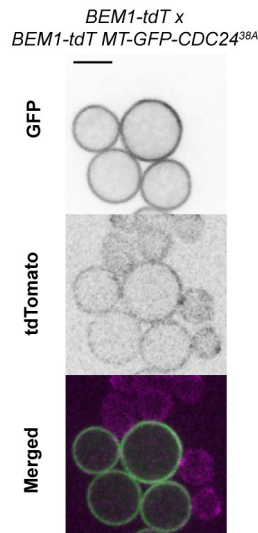


Figure 18: Overexpression of membrane-targeted Cdc24 blocks polarization. Medial plane confocal images of cells induced to express membrane-targeted, phospho-site mutant *GFP-CDC24^{38A}* (*MT-GFP-CDC24^{38A} BEM1-tdTomato*, DLY23351) and mixed with wildtype cells (*BEM1-tdTomato*, DLY12944).

Discussion

2.3.1 Exploratory polarization underlies partner selection in yeast mating

Our findings indicate that the transient polarity sites formed during the indecisive period are critical for subsequent commitment to a mating partner. Proteins involved in pheromone sensing, secretion, and signaling were all enriched at these sites, suggesting that they are preferred sites for both pheromone secretion and sensing. Wildtype cells in mating mixes did not commit to partners that lacked polarity sites, partners with constitutively mobile polarity sites, or partners with stable but misoriented polarity sites. These results are fully consistent with the exploratory polarization hypothesis (**Figure 5D**), in which transient polarity sites mediate communication between mating partners.

Previous findings indicated that the appearance of a strong, stable polarity site, which we call “commitment,” results from detection of a high concentration of pheromone (Hegemann et al., 2015; Henderson et al., 2019; McClure et al., 2015; Moore, 1983). Moreover, MAPK activity rises concomitant with commitment to a partner (Aymoz et al., 2018; Conlon et al., 2016; Henderson et al., 2019), consistent with the idea that cells sense higher levels of pheromone when their polarity sites align. Our findings suggest that pheromone levels sufficient to trigger commitment are only achieved when a partner’s polarity site is directly apposed to that in the receiving cell. Simulations confirm that local pheromone secretion would expose a well-oriented polarity site to much higher pheromone levels than those attainable by a cell secreting pheromone uniformly around its surface. Thus, yeast cells may commit to a partner in response to the concentrated pheromone signal that accompanies coorientation of the two cells’ polarity sites.

An open question concerns the mechanism whereby the two partner cells’ polarity sites “find each other” to become cooriented. One could imagine that polarity sites form, move, and disappear stochastically until coorientation promotes stable commitment, as proposed for “speed dating” in *S. pombe* (Bendezu and Martin, 2013; Merlini et al., 2016). Alternatively, polarity sites may be guided toward each other by pheromone gradients. Our simulations indicate that when pheromone is secreted

locally, the mating partner would experience a steep gradient in pheromone concentration, potentially guiding the movement or formation of polarity sites.

2.3.2 Re-evaluating the pheromone landscape of mating cells

The observation that yeast cells are able to orient polarization toward artificial pheromone sources generated by micropipets (Nern and Arkowitz, 1998; Segall, 1993; Valtz et al., 1995) or microfluidic devices (Brett et al., 2012; Dyer et al., 2013; Hao et al., 2008; Hegemann et al., 2015; Jin et al., 2011; Kelley et al., 2015; Lee et al., 2012; Moore et al., 2008; Moore et al., 2013; Paliwal et al., 2007; Vasen et al., 2020a) has focused attention on the mechanism whereby cells decode a stable gradient of pheromone. Although yeast cells are clearly capable of polarizing growth toward an exogenous pheromone source, wildtype cells failed to polarize growth toward partners that were secreting pheromone uniformly around their surface. As such cells would be expected to set up a stable pheromone gradient similar to that from a micropipet, why did their partners not commit?

Experiments that analyze polarization of **a** cells in artificial α -factor gradients generally focus on cells that remain arrested in G1 for prolonged periods (4-10 h). Cells that are further from the pheromone source arrest only transiently and then resume budding, and these cells are omitted from the analysis of directional polarization in the gradient. However, we suggest that this transiently arrested population may be the most relevant to the behavior of mating cells. For the **a** cells in our wildtype by wildtype

matings at 30°C, we found that 11% (n = 523 cells, 5 movies) of cells went on to bud during a 2 h observation window. Note that this analysis excludes cells that were not directly adjacent to (touching) potential G1-phase mating partners. Thus, cells that do not mate are unlikely to remain arrested in G1 for many hours under these circumstances. The simplest explanation for the failure of cells to commit to unpolarized partners is that yeast cells simply do not secrete enough pheromone to recreate the kinds of gradients produced by microfluidics devices.

Unlike experimental settings with unidirectional gradients, yeast cells in physiological mating scenarios must often discriminate between two or more similarly-distant pheromone sources (McClure et al., 2018; Taxis et al., 2005). Under those circumstances, stable pheromone gradients would seem unlikely, and the findings presented in this and other recent studies (Bendezu and Martin, 2013; Dyer et al., 2013; Henderson et al., 2019; Merlini et al., 2016; Wang et al., 2019) suggest that mating cells operate in the context of a fluctuating pheromone landscape quite unlike the stable gradients studied thus far. Fluctuations occur on several timescales. First, vesicular release of α -factor would generate dramatic sub-second spikes in pheromone concentration, because each vesicle contains very concentrated (~ 4 mM) α -factor. With an estimated α -factor diffusion constant of $150 \mu\text{m}^2/\text{s}$, each spike would dissipate to low nM levels well before the next spike, generating rapid fluctuations. Second, the movement of the polarity sites during the indecisive phase means that the source of

pheromone would relocate on a minute timescale, shifting the local gradients. Third, on a several-minute timescale, the mating or budding of nearby cells would remove them as pheromone sources in the local environment. Thus, physiological pheromone gradients are likely to be transitory, at least until the partners commit to each other. We suggest that the exploratory polarization strategy provides a framework for understanding how yeast cells are able to locate partners and mate successfully in such a dynamic pheromone landscape.

2.3.3 Advantages of exploratory polarization

The exploratory polarization strategy supported by our findings, like the related speed dating strategy proposed for *S. pombe* (Bendezu and Martin, 2013; Martin, 2019; Merlini et al., 2016), provides an elegant solution to the problem of choosing a partner from among two or more similarly-distant candidates. Classical spatial sensing paradigms that integrate spatial information to extract a single “up-gradient” direction are poorly suited to this task, as the presence of two or more nearby chemoattractant sources may create a weak or even non-existent net gradient. The task of picking just one of the potential partners is accomplished by the coincidence-detection feature of exploratory polarization: stabilization of the polarity site only occurs when the partners’ polarity sites happen to align (**Figure 5D**). By including this temporal aspect in the partner search process, the cells can avoid the potential paralysis that could ensue from access to two or more equally attractive partners. We note that this partner selection task

occurs not only in mating, but also more broadly in multicellular contexts that involve formation of focal cell-cell junctions like synapses.

A potential problem with exploratory polarization stems from the observation that during the indecisive phase, cells frequently developed two or more transient polarity sites. In principle, then, a cell could end up with two polarity sites each oriented toward a different partner, leading to double mating. However, cells avoid this problem due to the competition between polarity sites that is built into the cell polarity circuit (Robertson et al., in press; Wu et al., 2015). Because polarity factors are continually recruited into polarity clusters and then, after a few seconds, released back to the shared cytoplasm, states with more than one polarity site are transitory and only one polarity site can persist stably for long enough to promote fusion.

3. Materials and methods

3.1 Yeast strains and plasmids

Strains were constructed using standard molecular biology techniques. Yeast strains used in this study (**Table 1**) were generated in the YEF473 background (*his3-Δ200 leu2-Δ1 lys2-801 trp1-Δ63 ura3-52*) (Bi and Pringle, 1996), except DLY15660, which is in the 15D background (*ade1, his2, leu2-3, 112 trp1-1, ura3Δns*). The following alleles were previously described: *BEM1-GFP:LEU2* (Kozubowski et al., 2008), *BEM1-tdTomato:HIS3* (Howell et al., 2012), *SPA2-mCherry:KAN^R* (Howell et al., 2009), *GFP-SEC4:URA3* (Chen et al., 2012), *ura3:ste20(ΔCRIB):URA3* (Moran et al., 2019), *STE2-sfGFP:URA3* and *bar1Δ:URA3* (Henderson et al., 2019), *rsr1Δ:HIS3* (Schenkman et al., 2002), *STE5:GAL-STE5-CTM:GAL4BD-hER-VP16:LEU2* and *SPA2-mCherry:HYG^R* (McClure et al., 2015), *STE7(1-33)-NLS-NLS-mCherry:URA3* (Durandau et al., 2015), and *GAL1p-PSR1(1-28)-GFP-CDC24^{38A}:LEU2* (Woods et al., 2015).

The *sst2Δ:URA3* disruption was generated by the one-step PCR-based method (Baudin et al., 1993) using pRS306 as template.

WHI5-GFP:S.p.HIS5 (Doncic et al., 2011) and *STE6-sfGFP:KAN^R* were constructed using methods described previously (Longtine et al., 1998) with DLB52 (pFA6a-GFP(S65T)-S.p.HIS5MX6; Addgene plasmid #41598) and DLB4292 (pFA6a-link-*yoSuperfolderGFP-Kan*; Addgene plasmid #44901) as templates.

GFP-STE4 was constructed in the YEF background by a pop-in, pop-out strategy. First, *GFP-STE4* was PCR-amplified from a strain derived from RDY126 (Suchkov et al., 2010). This fragment was inserted into *pRS41N* (Taxis and Knop, 2006) using *ApaI* and *NotI*, producing DLB4171 (*pRS41N-GFP-STE4*). DLB4171 was digested with *HindIII* and *ApaI* to release a fragment containing the *STE4* promoter, GFP, and bp 1-194 of the ORF. This fragment was inserted into DLB212 (*pRSII306*: a *URA3*-marked integrating plasmid) to produce DLB4254 (*pRSII306-Ste4prom-GFP-Ste4(1-194)*). DLB4254 was partially digested with *PstI* to target integration to the *STE4* locus of a diploid from the YEF background. Haploid segregants containing *STE4(1-194)*, *URA3* marker, and *GFP-STE4* at the *STE4* locus were plated on medium containing 5-fluoroorotic acid to select for colonies in which recombination occurred between the promoter of the *STE4* fragment and the promoter of *GFP-STE4*, removing the *URA3* marker and leaving *GFP-STE4* as a precise replacement of the endogenous *STE4*.

To introduce the *cdc24-4* allele into the YEF473 strain background, we first deleted one copy of *CDC24* in a diploid strain using the *HIS3* marker. A centromeric *URA3*-marked plasmid carrying wildtype *CDC24* was transformed into the strain, and following sporulation and tetrad dissection a haploid *cdc24::HIS3* strain carrying the plasmid was selected. *cdc24-4* was amplified by PCR from a strain derived from JPT19-H01 (Sloat et al., 1981), and used to replace the *cdc24::HIS3* allele by homologous

recombination, followed by selection on medium containing 5-fluoroorotic acid to obtain colonies without the plasmid.

The *cdc24-m1* allele was amplified by PCR from *pRS414-cdc24-m1* (Nern and Arkowitz, 1998) and cloned into pRS306 to produce DLB4435 (*pRS306-cdc24-m1*). DLB4435 was digested with BspEI to target integration at the *CDC24* promoter, yielding a locus where the *URA3* gene is inserted between the *cdc24-m1* allele and wildtype *CDC24*. Haploid MATa segregants were grown on medium containing 5-fluoroorotic acid to select for recombination between *cdc24-m1* and *CDC24*. Recombinants containing *cdc24-m1* were identified by phenotyping (morphology when treated with pheromone) and confirmed by sequencing. To generate *cdc24-m1:TRP1*, DLB4287 containing a C-terminal fragment of *cdc24-m1* ORF and 501 bp of 3'-UTR in the pRS304 backbone (Sikorski and Hieter, 1989) was digested at the unique *XcmI* site in *cdc24-m1* to target integration at *CDC24*. This generates a tandem duplication with full-length *cdc24-m1* followed by *TRP1* and a promoterless truncated *CDC24* fragment.

3.2 Live-cell microscopy

Cells were grown in complete synthetic medium (CSM; MP Biomedicals, LLC, Solon, OH, USA) with 2% dextrose (Macron, Center Valley, PA, USA) overnight at 30°C to mid-log phase ($10^6 - 10^7$ cells/ml). Cultures of opposite mating type strains were mixed to obtain a 1:1 cell ratio, centrifuged to concentrate the cells, and mounted on CSM-dextrose slabs solidified with 2% agarose (Hoefer, Holliston, MA, USA) and sealed

with petroleum jelly. For pheromone “confusion” experiments, cells were imaged on a slab containing 10 μ M α -factor (Genway Biotech, San Diego, CA, USA). For uniform pheromone experiments, cells were imaged on a slab containing 5 nM α -factor. *GAL1p-MT-CDC24^{38A}* expression was induced in dextrose medium by adding β -estradiol (Sigma-Aldrich, St. Louis, MO, USA) to the medium to a final concentration of 20 nM, incubating for 2 h, and imaging on a slab containing 20 nM β -estradiol (the strains contain an artificial transcription factor, *GAL-4BD-hER-VP16*, that induces the *GAL1* promoter in response to β -estradiol). For *cdc24-4^{ts}* strains, cells were grown overnight at 24°C and shifted to 37°C for 2 h before imaging. For cells that were arrested in G1 (*MT-CDC24^{38A}* or *cdc24-4^{ts}*), α -factor was added to a final concentration of 10 μ M, and cells were incubated for 2 h before imaging on a slab containing 10 μ M α -factor. Imaging was performed in a temperature-controlled chamber at 30°C or the restrictive temperature as indicated.

Images were acquired with an Andor Revolution XD spinning disk confocal microscope (Andor Technology, Concord, MA, USA) with a CSU-X1 5,000-rpm confocal scanner unit (Yokogawa, Tokyo, Japan) and a UPLSAPO 100 \times /1.4 oil-immersion objective (Olympus, Tokyo, Japan), controlled by MetaMorph software (Molecular Devices, San Jose, CA, USA). Images were captured by an iXon3 897 EM-CCD camera with 1.2x auxiliary magnification (Andor Technology).

Images were acquired in z-stacks (15 0.47- μ m steps) at 2-min intervals. Laser power varied by experiment but was set to levels that produced bright signals with minimal bleaching during the movie: 8-15% (488 nm) and 10-15% (561 nm) of maximal output. EM gain was 200, and exposure time was 250 ms. Images were denoised with the ImageJ Hybrid 3D Median Filter plug-in (2007), created by Christopher Philip Mauer and Vytas Bindokas. Images are maximum projections except for *MT-CDC24^{38A}* medial plane image, as indicated. Scaling of images was always matched for experimental and relevant control conditions.

3.3 Scoring colocalization of *Ste2*, *Ste4*, *Ste6*, and *Sec4* with *Bem1*

Scoring was conducted in two steps: 1) Selection of scorable time points. From mating movies, we identified all cells in G1 that were adjacent to at least one potential G1-phase partner. Time points with 1 or 2 predominant Bem1 clusters or arcs/crescents were selected for scoring. Arcs or crescents of uneven intensity were considered a single continuous region. Time points where the Bem1 signal was dim, diffusely distributed, covered >50% of the cortex, appeared in >2 clusters, or could otherwise not be clearly localized to 1 or 2 distinct regions were excluded from scoring. Bem1 signal at the neck (cytokinesis or cytokinesis-remnant) was ignored, but neck-adjacent signal could be scored. Occasional tight puncta (<5 pixels) of Bem1 were also ignored. 2) Scoring colocalization. For each scorable time point, Bem1 and the protein of interest were considered colocalized if the signal of interest was more intense at/near the Bem1 signal

than in the broader neighborhood. Because some other probes localized to tighter foci than Bem1, complete overlap was not required to score an image as colocalized. Signals at other, non-colocalized regions were also allowed. For time points with 2 comparable Bem1 clusters, overlap with either cluster was scored as colocalization. For time points with 2 unequal clusters, overlap with the more prominent cluster was required to score colocalization. Because Ste2-sfGFP often accumulated on the plasma membrane as a crescent, a region of Ste2 was judged to be colocalized only if the more intense part of the crescent overlapped with the Bem1 cluster. To minimize inherent subjectivity, cases judged ambiguous by the rater were excluded.

3.4 Mating efficiency

Mating efficiencies were calculated from mating movies. We tracked all cells in G1 that were adjacent to at least one potential G1-phase partner (i.e., “available” to mate) during a 2-h movie and scored them as “mated” or “not mated.” Cells whose potential partners mated with another cell and cells that were available to mate only during the last 20 min were excluded from the sample.

3.5 Budding index

Budding indices were calculated from mating movies. Using the appearance of Bem1-GFP or Bem1-tdTomato at the neck as a marker of G1, we first calculated the duration of G1 for all wildtype α -cells that mated (mutants were **a**-cells) and determined the median of that value (52 min). We then tracked all cells in G1 that were adjacent to at

least one potential G1-phase partner (i.e., “available” to mate) for 52 min, noting whether they budded, mated, or remained arrested.

3.6 Halo assays to measure pheromone secretion

a-factor pheromone promotes G1 arrest of MAT α cells, while α -factor pheromone promotes G1 arrest of MAT \mathbf{a} cells. Halo assays detect the pheromone produced by a spot of cells placed on a lawn of supersensitive cells of the opposite mating type. Lawns (3.5×10^6 cells) were spread on YEPD plates (1% yeast extract, 2% peptone, 2% dextrose). Lawn strains were DLY8993 (MAT \mathbf{a} *bar1* Δ) to detect α -factor and DLY15660 (MAT α *ssf2* Δ) to detect **a**-factor. After spreading the lawn on the plate and allowing it to dry, spots containing 10^7 cells of the strains to be tested were pipetted onto the lawn. Halos (zones of G1 arrest) were photographed after 48 h at 30°C. Because cells make more pheromone when they are in G1 phase (Henderson et al., 2019), we performed similar assays using cells that were arrested in G1 by expression of Ste5-CTM (Pryciak and Huntress, 1998). Expression was induced by addition of 300 nM β -estradiol to the plate. Halo diameter was quantified by fitting a circle to each halo.

3.7 Spatial autocorrelation analysis

The image processing toolbox in MATLAB 2019a was used to develop a custom tool to track individual cells during the mating period and determine commitment to a partner in an unbiased way. From mating movies, we identified wildtype α -cells (*BEM1-GFP* or *BEM1-tdTomato*) that were available to mate with **a**-cell partners. We

circumscribed the wildtype cells at several time points throughout the movie, beginning at G1 and ending either at the time point preceding fusion (for cells that mated) or the end of the movie (for cells that did not mate). Using linear interpolation, the outlines were deformed over time to accommodate changes in cell morphology and position. In this manner, we obtained cell outlines between the marked time points, enabling continuous tracking of each cell during the mating period.

The spatial array of intracellular Bem1 signal was extracted at each time point, and the correlation between arrays at adjacent time points was calculated (“spatial autocorrelation”), using the following formula:

$$r(t) = \frac{\text{cov}(C(t), C(t + 1))}{\sigma_{C(t)}\sigma_{C(t+1)}}$$

where r is Pearson’s coefficient, cov is covariance, C is an array containing indexed fluorescence data, t is time point, and σ_C is the standard deviation of the array C . The two arrays $C(t)$ and $C(t + 1)$ were obtained by using a union of the outlines at time points t and $t + 1$ to ensure that spatial overlap was continuous.

During the indecisive period, r is relatively low, but at commitment, r is relatively high.

To determine a threshold of r that indicates commitment, we performed a sweep

through different threshold values for a set of cells for which an experienced rater had already judged the time of commitment. A threshold value was selected to minimize discrepancies (either early or late judgments) between the automated and the human rater. We note that different thresholds were selected for different probes (GFP or tdTomato) and different temperatures to account for imaging variations. The code used for this analysis can be found at: <https://github.com/DebrajGhose/Exploratory-polarization-yeast>

3.8 Calculation of pheromone concentrations expected for global and local secreting cells

To gain insight into the types of gradients expected from global and local secreting cells, we considered the gradient generated by a spherical emitter centered at the origin (Rappaport and Barkai, 2012). For this case, the pheromone gradient can be found by solving Laplace's equation using spherical coordinates. The r-coordinate satisfies the equation:

$$\frac{\partial \left(\frac{r^2 \partial C}{\partial r} \right)}{\partial r} = 0$$

The boundary conditions are constant flux density J (number of molecules released per unit time per unit area) at the surface of the sphere ($r = R$)

$$-D \left[\frac{\partial C}{\partial r} \right]_{r=R} = J$$

and the concentration vanishes as $r \rightarrow \infty$. With these boundary conditions, the concentration takes the following form:

$$C(r) = \frac{JR^2}{D r}$$

In terms of the total secretion rate S , the above expression becomes

$$C(r) = \frac{\left(\frac{S}{4\pi R^2} \right) R^2}{D r} = \frac{S}{4\pi D r}$$

If we assume a secretion rate of 1400 molecules/s and diffusion coefficient for pheromone molecules of $150 \mu\text{m}^2/\text{s}$, then the concentration at the surface of cell of radius $2.5 \mu\text{m}$ is $C(2.5) = 0.3 \text{ molecules}/\mu\text{m}^3 = 0.5 \text{ nM}$. If we assume the localized emitter has a radius of $0.25 \mu\text{m}$, then the concentration at the surface of the emitter is 10 times higher $C(0.25) = 5 \text{ nM}$. These results are consistent with the emitter alone results shown in **Figure 9B**.

3.9 Simulations of pheromone landscape for two touching cells

Particle-based simulations of pheromone emission and diffusion were conducted using the Smoldyn software (v2.58) on Linux systems (2.50 GHz and 2.30 GHz Intel processors, Longleaf cluster at UNC Chapel Hill, NC, USA (Andrews, 2017; Andrews

and Bray, 2004). Code is available at <https://github.com/mikepab/exploratory-polarization-yeast>. Pheromone molecules were modeled as Brownian point particles with diffusion coefficient $D = 150 \mu\text{m}^2/\text{s}$, and were removed at a spherical absorbing boundary $50 \mu\text{m}$ from the origin. A mating pair was modeled as a two spheres, a receiver and emitter, centered at $(\pm(2.5+0.25/2) \mu\text{m}, 0 \mu\text{m}, 0 \mu\text{m})$ with radius $2.5 \mu\text{m}$. The system was first equilibrated for 5 seconds, after which coordinates were recorded every 0.1 ms timestep for 10 seconds. For each condition, $n = 300$ realizations were conducted.

Vesicle emission events were simulated by repeated use of the Smoldyn command `cmd @ t pointsource pheromone n x y z`. First, t specifies the time of a single emission event; intervals between each emission were exponentially distributed:

$$t_k = \sum_{i=0}^k \tau_i \text{ for } \tau \sim \text{Exponential}(1.188 \text{ s}^{-1})$$

pheromone is a molecular species defined in the Smoldyn script, n is the number of molecules released per vesicle ($n = 1663$), and $x y z$ are spatial coordinates of the vesicle event. In the local case, $(x = -0.25/2+0.001 \mu\text{m}, y = z = 0 \mu\text{m})$. In the global case, the spatial coordinates were obtained by uniform random sampling on a sphere centered at $(-(2.5+0.25/2) \mu\text{m}, 0 \mu\text{m}, 0 \mu\text{m})$ with radius $2.5001 \mu\text{m}$.

Single-molecule emission events were handled using the Smoldyn reaction `surface=` and `reaction_production` commands, with a release rate per timestep of $1/7.1429$ (yielding 1400 molecules per second at 0.1 ms timesteps). In the local case, the

releasing surface was a sphere centered at $x = -0.25/2+0.001 \mu\text{m}$, $y = z = 0 \mu\text{m}$ with a radius of $0.0005 \mu\text{m}$. In the global case, the releasing surface was a sphere centered at $(- (2.5+0.25/2), 0, 0) \mu\text{m}$ with radius $2.5001 \mu\text{m}$.

To validate the simulation setup, we set up simulations comparable to the analytic solution described above. The receiver was removed, and pheromone profiles were measured as a function of distance to the emitter. The simulations were in good agreement with the analytic solution (**Figure 9B**).

3.10 Analysis of particle-based pheromone simulations

Receiver-centered molecular coordinates were filtered to only include pheromone within $0.25 \mu\text{m}$ of the receiver surface. Then, a 3D angle between each molecule \vec{r}_i and a reference vector (\vec{v}) was calculated:

$$\theta_i = \arccos\left(\frac{\vec{r}_i \cdot \vec{v}}{\|\vec{r}_i\| \|\vec{v}\|}\right)$$

The reference vector defines the patch under consideration (**Figure 9A**). For 0° , the closest patch to the emitter $\vec{v} = [-1,0,0]$. For the other patches, we rotate $[-1,0,0]$ by the desired angle θ_{rot} .

$$\vec{v} = \begin{bmatrix} \cos(\theta_{rot}) & -\sin(\theta_{rot}) & 0 \\ \sin(\theta_{rot}) & \cos(\theta_{rot}) & 0 \\ 0 & 0 & 1 \end{bmatrix} \times \begin{bmatrix} -1 \\ 0 \\ 0 \end{bmatrix}$$

To count molecules in each patch, we summed the number of points within $0^\circ \leq \theta_i \leq 30^\circ$. The volume of each patch is $V = \frac{2\pi}{3} (2.75^3 - 2.5^3) \left(1 - \cos\left(\frac{\pi}{6}\right)\right)$, which was used to convert molecules to nanomolar. Finally, a time-averaged pheromone concentration and coefficient of variation (CV) were calculated for each patch in each simulation, allowing us to compute a mean and standard error across simulations (**Figure 8D-G**).

3.11 Yeast and plasmid strains and genotypes

Table 1: Yeast strains and genotypes

Yeast strain	Relevant genotype	Source
DLY8503	<i>MATα SPA2-mCherry:KAN^R</i>	This study
DLY8993	<i>MATα bar1:URA3</i>	(Henderson et al., 2019)
DLY9069	<i>MATα BEM1-GFP:LEU2</i>	(Howell et al., 2009)
DLY9070	<i>MATα BEM1-GFP:LEU2</i>	(Kozubowski et al., 2008)
DLY12943	<i>MATα BEM1-tdTomato:HIS3</i>	(Henderson et al., 2019)
DLY12944	<i>MATα BEM1-tdTomato:HIS3</i>	This study
DLY13771	<i>MATα BEM1-tdTomato:HIS3 ura3:GFP-SEC4:URA3</i>	(Henderson et al., 2019)
DLY15660	<i>MATα sst2:URA3</i>	This study
DLY20625	<i>MATα SPA2-mCherry:KAN^R STE5:GAL-STE5-CTM:GAL4BD- hER-VP16:LEU2</i>	This study
DLY20628	<i>MATα SPA2-mCherry:KAN^R WHI5- GFP:HIS5 STE5:GAL-STE5- CTM:GAL4BD-hER-VP16:LEU2</i>	This study
DLY20712	<i>MATα SPA2-mCherry:KAN^R STE2- sfGFP:URA3</i>	This study
DLY22243	<i>MATα BEM1-tdTomato:HIS3 STE2- sfGFP:URA3</i>	(Henderson et al., 2019)
DLY22340	<i>MATα BEM1-tdTomato:HIS3</i>	(Henderson et al., 2019)

DLY22355	<i>MATa</i> BEM1-tdTomato STE6-sfGFP:KAN ^R	This study
DLY22532	<i>MATa</i> SPA2-mCherry:KAN ^R WHI5-GFP:HIS5 STE5:GAL-STE5-CTM:GAL4BD-hER-VP16:LEU2 <i>cdc24-m1</i> :TRP1 <i>rsr1Δ</i> :HIS3	This study
DLY22533	<i>MATα</i> SPA2-mCherry:HYG ^R STE5:GAL-STE5-CTM:GAL4BD-hER-VP16:LEU2 <i>cdc24-m1</i> :TRP1 <i>rsr1Δ</i> :HIS3	This study
DLY22797	<i>MATa</i> BEM1-GFP:LEU2 <i>cdc24-m1</i> (unmarked) <i>rsr1Δ</i> :HIS3	This study
DLY23016	<i>MATa</i> BEM1-GFP:LEU2 STE7(1-33)-NLS-NLS-mCherry:URA3 <i>bar1::URA3</i>	This study
DLY23256	<i>MATa</i> BEM1-tdTomato:HIS3 <i>ura3:ste20(ΔCRIB)</i> :URA3 <i>cdc24-4^{ts}</i> (unmarked) WHI5-GFP:HIS5	This study
DLY23351	<i>MATa</i> BEM1-tdTomato:HIS3 GAL1p-PSR1(1-28)-GFP-CDC24 ^{38A} :LEU2 GAL-4BD-hER-VP16:URA3 WHI5-GFP:HIS5	This study
DLY23354	<i>MATα</i> BEM1-tdTomato:HIS3 GFP-STE4 (unmarked)	This study
DLY23612	<i>MATα</i> BEM1-GFP:LEU2 <i>cdc24-m1</i> (unmarked) <i>rsr1Δ</i> :HIS3	This study

Table 2: Plasmid strains and genotypes

Plasmid	Relevant genotype	Source
DLB52	<i>pFA6a-GFP(S65T)-HIS3MX6</i>	(Bähler et al., 1998)
DLB3156	<i>pRS414cdc24-m1</i>	(Nern and Arkowitz, 1998)
DLB4171	<i>pRS41N-GFP-STE4</i>	This study
DLB4254	<i>pRSII306-Ste4prom-GFP-Ste4(1-194)</i>	This study
DLB4292	<i>pFA6a-link-yoSuperfolderGFP-Kan</i>	(Lee et al., 2013)
DLB4435	<i>pRS306-cdc24-m1:URA3</i>	This study
DLB4287	<i>pRS304-cdc24-m1-C:TRP1</i>	This study

4. Conclusions

4.1 Conclusions

This study provides experimental evidence for the exploratory model of polarization in budding yeast during mating. According to this model (**Figure 5D**), in a mating mix, cells respond to low-dose pheromone by forming polarity sites that appear at different places on the cell cortex over time during an indecisive period. These polarity sites are often enriched in pheromone receptors, $G\beta\gamma$, and markers of pheromone secretion, indicating that they could mediate local pheromone sensing and secretion.

Computational modeling of two nearby cells (a pheromone emitter and a receiver) shows how the location and manner of secretion by one affect the pheromone concentration sensed by the other. When the two polarity sites are opposite each other and the emitter secretes locally (i.e., from its polarity site), the concentration of pheromone at the receiver's polarity site is approximately 8x that experienced if the emitter secretes globally (i.e., all over its surface). This is only true if the two sites are aligned. The concentration at the receiver's polarity site drops off sharply as the emitter's polarity site is more distant from it. Therefore, if sensing a concentrated dose of pheromone is critical for a cell to commit to a partner, then a signal secreted at the polarity site would be more likely to release sufficient pheromone to stabilize its partner's polarity site than a globally-released signal.

Mating experiments between wildtype cells and mutants that lack the ability to make stable polarity sites show that the latter are markedly deficient at stably attracting a mating partner. This is true whether the cells make no polarity sites or make constitutively mobile sites that cannot stabilize opposite a partner. In the latter case, I observed no successful mating events, and in the former, I observed mating <1% of the time (compared with mating 60-70% of the time in wildtype x wildtype pairs. Together, these data suggest that only cells that can stably secrete toward a partner will efficiently attract that partner as a mate.

This observation also explains how cells treated with high-dose pheromone can mate (albeit at reduced efficiency) despite being unable to search. Live-cell imaging of mating attempts between searching cells and “confused” partners revealed that the searching cell only committed to a partner that oriented secretion toward it by chance. Therefore, non-chemotropic mating can occur, provided one partner is able to search. This model might offer insight into non-chemotropic mating in other fungi, such as clonal mating seen in *C. neoformans*.

4.2 Future directions

4.2.1 How do two polarity sites become aligned?

One important mechanistic question is how two polarity sites become aligned. One possibility is a completely random search in which encounters are stochastic. Another is a directed search in which a patch is more likely to move toward another

patch than toward a region without a partner's patch. A recent study found that cells place their initial patches toward the eventual mating partner at better than chance frequencies, suggesting that they are able to take some measurement of the landscape before polarity sites are visible on the cortex (Henderson et al., 2019). Therefore, global sensing strategies appear to play some role in initial polarity site orientation. Whether they also contribute to the polarity site's trajectory during the search remains to be determined. It is also possible that both random and directed movements play roles at different parts of the search or under different conditions.

4.2.2 Is polarized sensing critical for chemotropism?

This study focused the signal that is required for a partner to become committed to a wildtype cell but did not test the importance of polarized sensing. Although there is evidence that when both receptors and $G\beta\gamma$ are unpolarized, the cell is unable to stabilize its polarity site, this experiment was performed in cells lacking $G\alpha$ (McClure et al., 2015). Therefore, it is impossible to attribute the defect solely to the unpolarized receptors and $G\beta\gamma$. The identification of a mutant in $G\beta$ or its associated subunits $G\alpha$ or $G\gamma$ that cause $G\beta$ to fail to polarize would allow more rigorous testing of this hypothesis. However, since the G proteins are thought to remain associated with each other throughout the mating process (Strickfaden and Pryciak, 2008), it might prove difficult to find a mutant with both unpolarized $G\beta\gamma$ and wildtype $G\alpha$ localization/function.

Another strategy for uncoupling polarized sensing and secretion is to disrupt polarized secretion without altering other aspects of polarity. α -factor is secreted by a dedicated transporter, Ste6. A particularly elegant way to test the importance of polarized secretion would be to identify a mutant with unpolarized Ste6 and ask if a wildtype partner could find and commit to it. Although a series of Ste6 internalization mutants were previously identified (Kelm et al., 2004), we found that on treatment with α -factor, these cells still polarized Ste6.

4.2.3 How does concentrated pheromone raise MAPK levels?

In wildtype cells, two apposed polarity sites appear to trigger a sharp increase in MAPK signaling that remains high until the two cells fuse (Henderson et al., 2019). Since concentrated pheromone stabilizes a mobile polarity site, the increase in MAPK is presumably the consequence of a concentrated pheromone signal. However, exactly how concentrated pheromone raises MAPK levels is unclear.

Attempts to answer this question by analyzing the MAPK profile of wildtype cells attempting to mate with the polarity mutants tested in this study were unsuccessful for technical reasons. Because the MAPK sensor signal varies from cell to cell, data from wildtype cells were normalized between the minimum and maximum of MAPK activity in mating cells (when the cell entered G1 and when it fused, respectively) (Henderson et al., 2019). However, cells in the present study rarely mated, and without this maximum value, the signal could not be normalized.

One alternative is to track the MAPK profile of cells with mild mating impairments. Preliminary studies indicate several possibilities: cells lacking the Rsr1 pathway appear to mate with lower efficiency than wildtype, and the fusion mutants *fus1Δ* and *fus2Δ* remain often remain committed to partners without mating. In both cases, the phenotype is variable within a population, such that differences in MAPK activity between successful and unsuccessful maters might be revealed.

4.2.4 Does the presence of the Ras-GTPase Rsr1 help or confuse cells during mating?

The Rsr1 pathway can provide positive feedback to stabilize a polarity site near the previous bud site after pheromone treatment. However, in mating mixes, the external pheromone cue appears to override the internal Rsr1 cue, and cells are not restricted to mating where they would have budded. Although not generally believed to be required for efficient mating (Nern and Arkowitz, 1999), the role of Rsr1 in chemotropism is disputed (Vasen et al., 2020a; Vasen et al., 2020b). Given that Rsr1 can be invoked as a polarity cue in the presence of pheromone, how does this cell override this information?

References

- Adams, A.E., D.I. Johnson, R.M. Longnecker, B.F. Sloat, and J.R. Pringle. 1990. CDC42 and CDC43, two additional genes involved in budding and the establishment of cell polarity in the yeast *Saccharomyces cerevisiae*. *The Journal of cell biology*. 111:131-142.
- Adler, J. 1975. Chemotaxis in bacteria. *Annual Review of Biochemistry*. 44:341-356.
- Alby, K., and R.J. Bennett. 2011. Interspecies pheromone signaling promotes biofilm formation and same-sex mating in *Candida albicans*. *Proceedings of the National Academy of Sciences of the United States of America*. 108:2510-2515.
- Alby, K., D. Schaefer, and R.J. Bennett. 2009. Homothallic and heterothallic mating in the opportunistic pathogen *Candida albicans*. *Nature*. 460:890-893.
- Andrews, S.S. 2017. Smoldyn: particle-based simulation with rule-based modeling, improved molecular interaction and a library interface. *Bioinformatics*. 33:710-717.
- Andrews, S.S., and D. Bray. 2004. Stochastic simulation of chemical reactions with spatial resolution and single molecule detail. *Phys Biol*. 1:137-151.
- Arkowitz, R., and M. Bassilana. 2019. Recent advances in understanding *Candida albicans* hyphal growth. *F1000Research*. 8.
- Arkowitz, R.A. 1999. Responding to attraction: Chemotaxis and chemotropism in *Dictyostelium* and yeast. *Trends in cell biology*. 9:20-27.
- Arkowitz, R.A. 2009. Chemical gradients and chemotropism in yeast. *Cold Spring Harbor perspectives in biology*. 1:a001958.
- Artemenko, Y., T.J. Lampert, and P.N. Devreotes. 2014. Moving towards a paradigm: Common mechanisms of chemotactic signaling in *Dictyostelium* and mammalian leukocytes. *Cellular and molecular life sciences : CMLS*. 71:3711-3747.
- Atkins, B.D., S. Yoshida, K. Saito, C.F. Wu, D.J. Lew, and D. Pellman. 2013. Inhibition of Cdc42 during mitotic exit is required for cytokinesis. *The Journal of cell biology*. 202:231-240.
- Aymoz, D., C. Solé, J.J. Pierre, M. Schmitt, E. de Nadal, F. Posas, and S. Pelet. 2018. Timing of gene expression in a cell-fate decision system. *Mol Syst Biol*. 14:e8024.

- Ayscough, K.R., and D.G. Drubin. 1998. A role for the yeast actin cytoskeleton in pheromone receptor clustering and signalling. *Current biology : CB*. 8:927-930.
- Bähler, J., J.Q. Wu, M.S. Longtine, N.G. Shah, A. McKenzie, 3rd, A.B. Steever, A. Wach, P. Philippsen, and J.R. Pringle. 1998. Heterologous modules for efficient and versatile PCR-based gene targeting in *Schizosaccharomyces pombe*. *Yeast (Chichester, England)*. 14:943-951.
- Bajaj, A., A. Celić, F.X. Ding, F. Naider, J.M. Becker, and M.E. Dumont. 2004. A fluorescent alpha-factor analogue exhibits multiple steps on binding to its G protein coupled receptor in yeast. *Biochemistry*. 43:13564-13578.
- Baudin, A., O. Ozier-Kalogeropoulos, A. Denouel, F. Lacroute, and C. Cullin. 1993. A simple and efficient method for direct gene deletion in *Saccharomyces cerevisiae*. *Nucleic acids research*. 21:3329-3330.
- Bauman, P., and C.F. Albright. 1998. Functional analysis of domains in the Byr2 kinase. *Biochimie*. 80:621-625.
- Bellon, A., and F. Mann. 2018. Keeping up with advances in axon guidance. *Current opinion in neurobiology*. 53:183-191.
- Bender, A., and J.R. Pringle. 1989. Multicopy suppression of the cdc24 budding defect in yeast by CDC42 and three newly identified genes including the ras-related gene RSR1. *Proceedings of the National Academy of Sciences*. 86:9976-9980.
- Bendezu, F.O., and S.G. Martin. 2013. Cdc42 explores the cell periphery for mate selection in fission yeast. *Current biology : CB*. 23:42-47.
- Bennett, R.J., and A.D. Johnson. 2006. The role of nutrient regulation and the Gpa2 protein in the mating pheromone response of *C. albicans*. *Molecular Microbiology*. 62:100-119.
- Bennett, R.J., and B.G. Turgeon. 2016. Fungal Sex: The Ascomycota. *Microbiology Spectrum*. 4.
- Bi, E., and J.R. Pringle. 1996. ZDS1 and ZDS2, genes whose products may regulate Cdc42p in *Saccharomyces cerevisiae*. *Molecular and cellular biology*. 16:5264-5275.
- Brett, M.E., R. DeFlorio, D.E. Stone, and D.T. Eddington. 2012. A microfluidic device that forms and redirects pheromone gradients to study chemotropism in yeast. *Lab Chip*. 12:3127-3134.

- Bui, T., X. Lin, R. Malik, J. Heitman, and D. Carter. 2008. Isolates of *Cryptococcus neoformans* from infected animals reveal genetic exchange in unisexual, alpha mating type populations. *Eukaryotic cell*. 7:1771-1780.
- Butty, A.C., P.M. Pryciak, L.S. Huang, I. Herskowitz, and M. Peter. 1998. The role of Far1p in linking the heterotrimeric G protein to polarity establishment proteins during yeast mating. *Science*. 282:1511-1516.
- Cai, H., and P.N. Devreotes. 2011. Moving in the right direction: How eukaryotic cells migrate along chemical gradients. *Seminars in Cell & Developmental Biology*. 22:834-841.
- Casadevall, A. 2019. Global catastrophic threats from the fungal kingdom. In *Global Catastrophic Biological Risks*. T.V. Inglesby and A.A. Adalja, editors. Springer International Publishing, Cham. 21-32.
- Chant, J., and I. Herskowitz. 1991. Genetic control of bud site selection in yeast by a set of gene products that constitute a morphogenetic pathway. *Cell*. 65:1203-1212.
- Chen, H., C.C. Kuo, H. Kang, A.S. Howell, T.R. Zyla, M. Jin, and D.J. Lew. 2012. Cdc42p regulation of the yeast formin Bni1p mediated by the effector Gic2p. *Molecular biology of the cell*. 23:3814-3826.
- Coelho, M.A., G. Bakkeren, S. Sun, M.E. Hood, and T. Giraud. 2017. Fungal Sex: The Basidiomycota. *Microbiology Spectrum*. 5.
- Conlon, P., R. Gelin-Licht, A. Ganesan, J. Zhang, and A. Levchenko. 2016. Single-cell dynamics and variability of MAPK activity in a yeast differentiation pathway. *Proceedings of the National Academy of Sciences of the United States of America*. 113:E5896-e5905.
- Cross, F., L.H. Hartwell, C. Jackson, and J.B. Konopka. 1988. Conjugation in *Saccharomyces cerevisiae*. *Annual review of cell biology*. 4:429-457.
- Dettmann, A., J. Illgen, S. März, T. Schürg, A. Fleissner, and S. Seiler. 2012. The NDR kinase scaffold HYM1/MO25 Is Essential for MAK2 MAP kinase signaling in *Neurospora crassa*. *PLoS genetics*. 8:e1002950.
- Doehlemann, G., B. Ökmen, W. Zhu, and A. Sharon. 2017. Plant pathogenic fungi. *Microbiology Spectrum*. 5.

- Dohlman, H.G., and J.W. Thorner. 2001. Regulation of G protein-initiated signal transduction in yeast: Paradigms and principles. *Annu Rev Biochem.* 70:703-754.
- Doncic, A., M. Falleur-Fettig, and Jan M. Skotheim. 2011. Distinct interactions select and maintain a specific cell fate. *Molecular cell.* 43:528-539.
- Dorer, R., C. Boone, T. Kimbrough, J. Kim, and L.H. Hartwell. 1997. Genetic analysis of default mating behavior in *Saccharomyces cerevisiae*. *Genetics.* 146:39-55.
- Dorer, R., P.M. Pryciak, and L.H. Hartwell. 1995. *Saccharomyces cerevisiae* cells execute a default pathway to select a mate in the absence of pheromone gradients. *The Journal of cell biology.* 131:845-861.
- Durandau, E., D. Aymoz, and S. Pelet. 2015. Dynamic single cell measurements of kinase activity by synthetic kinase activity relocation sensors. *BMC Biol.* 13:55.
- Dyer, J.M., N.S. Savage, M. Jin, T.R. Zyla, T.C. Elston, and D.J. Lew. 2013. Tracking shallow chemical gradients by actin-driven wandering of the polarization site. *Current biology : CB.* 23:32-41.
- Fleissner, A., A.C. Leeder, M.G. Roca, N.D. Read, and N.L. Glass. 2009. Oscillatory recruitment of signaling proteins to cell tips promotes coordinated behavior during cell fusion. *Proceedings of the National Academy of Sciences.* 106:19387.
- Fones, H.N., M.C. Fisher, and S.J. Gurr. 2017. Emerging fungal threats to plants and animals challenge agriculture and ecosystem resilience. *Microbiology Spectrum.* 5.
- Fraser, J.A., S.S. Giles, E.C. Wenink, S.G. Geunes-Boyer, J.R. Wright, S. Diezmann, A. Allen, J.E. Stajich, F.S. Dietrich, J.R. Perfect, and J. Heitman. 2005. Same-sex mating and the origin of the Vancouver Island *Cryptococcus gattii* outbreak. *Nature.* 437:1360-1364.
- Fukui, Y., and M. Yamamoto. 1988. Isolation and characterization of *Schizosaccharomyces pombe* mutants phenotypically similar to *ras1*⁻. *Molecular and General Genetics MGG.* 215:26-31.
- Gammie, A.E., V. Brizzio, and M.D. Rose. 1998. Distinct morphological phenotypes of cell fusion mutants. *Molecular biology of the cell.* 9:1395-1410.
- Glass, N.L., S.J. Vollmer, C. Staben, J. Grotelueschen, R.L. Metzberg, and C. Yanofsky. 1988. DNAs of the two mating-type alleles of *Neurospora crassa* are highly dissimilar. *Science.* 241:570+.

- Guan, G., L. Tao, H. Yue, W. Liang, J. Gong, J. Bing, Q. Zheng, A.O. Veri, S. Fan, N. Robbins, L.E. Cowen, and G. Huang. 2019. Environment-induced same-sex mating in the yeast *Candida albicans* through the Hsf1–Hsp90 pathway. *PLoS Biol.* 17:e2006966.
- Haber, J.E. 2012. Mating-type genes and MAT switching in *Saccharomyces cerevisiae*. *Genetics.* 191:33-64.
- Hao, N., S. Nayak, M. Behar, R.H. Shanks, M.J. Nagiec, B. Errede, J. Hasty, T.C. Elston, and H.G. Dohlman. 2008. Regulation of cell signaling dynamics by the protein kinase-scaffold Ste5. *Molecular cell.* 30:649-656.
- Hegemann, B., and M. Peter. 2017. Local sampling paints a global picture: Local concentration measurements sense direction in complex chemical gradients. *BioEssays : news and reviews in molecular, cellular and developmental biology.* 39.
- Hegemann, B., M. Unger, Sung S. Lee, I. Stoffel-Studer, J. van den Heuvel, S. Pelet, H. Koepl, and M. Peter. 2015. A cellular system for spatial signal decoding in chemical gradients. *Developmental cell.* 35:458-470.
- Henderson, N.T., M. Pablo, D. Ghose, M.R. Clark-Cotton, T.R. Zyla, J. Nolen, T.C. Elston, and D.J. Lew. 2019. Ratiometric GPCR signaling enables directional sensing in yeast. *PLoS Biol.* 17:e3000484-e3000484.
- Herzog, S., M.R. Schumann, and A. Fleißner. 2015. Cell fusion in *Neurospora crassa*. *Current Opinion in Microbiology.* 28:53-59.
- Higashiyama, T., and H. Takeuchi. 2015. The mechanism and key molecules involved in pollen tube guidance. *Annual review of plant biology.* 66:393-413.
- Howell, Audrey S., M. Jin, C.-F. Wu, Trevin R. Zyla, Timothy C. Elston, and Daniel J. Lew. 2012. Negative feedback enhances robustness in the yeast polarity establishment circuit. *Cell.* 149:322-333.
- Howell, A.S., N.S. Savage, S.A. Johnson, I. Bose, A.W. Wagner, T.R. Zyla, H.F. Nijhout, M.C. Reed, A.B. Goryachev, and D.J. Lew. 2009. Singularity in polarization: Rewiring yeast cells to make two buds. *Cell.* 139:731-743.
- Hull, C.M., and J. Heitman. 2002. Genetics of *Cryptococcus neoformans*. *Annual Review of Genetics.* 36:557-615.

- Irazoqui, J.E., A.S. Gladfelter, and D.J. Lew. 2003. Scaffold-mediated symmetry breaking by Cdc42p. *Nature cell biology*. 5:1062-1070.
- Ismael, A., and D.E. Stone. 2017. Yeast chemotropism: A paradigm shift in chemical gradient sensing. *Cellular logistics*. 7:e1314237.
- Jackson, C.L., and L.H. Hartwell. 1990a. Courtship in *S. cerevisiae*: Both cell types choose mating partners by responding to the strongest pheromone signal. *Cell*. 63:1039-1051.
- Jackson, C.L., and L.H. Hartwell. 1990b. Courtship in *Saccharomyces cerevisiae*: An early cell-cell interaction during mating. *Molecular and cellular biology*. 10:2202-2213.
- Jenness, D.D., A.C. Burkholder, and L.H. Hartwell. 1983. Binding of α -factor pheromone to yeast a cells: Chemical and genetic evidence for an α -factor receptor. *Cell*. 35:521-529.
- Jenness, D.D., and P. Spatrack. 1986. Down regulation of the α -factor pheromone receptor in *S. cerevisiae*. *Cell*. 46:345-353.
- Jin, M., B. Errede, M. Behar, W. Mather, S. Nayak, J. Hasty, H.G. Dohlman, and T.C. Elston. 2011. Yeast dynamically modify their environment to achieve better mating efficiency. 4:ra54-ra54.
- Johnson, J.M., M. Jin, and D.J. Lew. 2011. Symmetry breaking and the establishment of cell polarity in budding yeast. *Current opinion in genetics & development*. 21:740-746.
- Jonkers, W., A.C. Leeder, C. Ansong, Y. Wang, F. Yang, T.L. Starr, D.G. Camp, II, R.D. Smith, and N.L. Glass. 2014. HAM-5 functions as a MAP kinase scaffold during cell fusion in *Neurospora crassa*. *PLoS genetics*. 10:e1004783.
- Kelley, J.B., G. Dixit, J.B. Sheetz, S.P. Venkatapurapu, T.C. Elston, and H.G. Dohlman. 2015. RGS proteins and septins cooperate to promote chemotropism by regulating polar cap mobility. *Current biology : CB*. 25:275-285.
- Kelm, K.B., G. Huyer, J.C. Huang, and S. Michaelis. 2004. The internalization of yeast Ste6p follows an ordered series of events involving phosphorylation, ubiquitination, recognition and endocytosis. *Traffic*. 5:165-180.

- Kim, H., and K.A. Borkovich. 2004. A pheromone receptor gene, *pre-1*, is essential for mating type-specific directional growth and fusion of trichogynes and female fertility in *Neurospora crassa*. *Molecular Microbiology*. 52:1781-1798.
- Kim, H., and K.A. Borkovich. 2006. Pheromones are essential for male fertility and sufficient to direct chemotropic polarized growth of trichogynes during mating in *Neurospora crassa*. *Eukaryotic cell*. 5:544-554.
- Kim, H., S.J. Wright, G. Park, S. Ouyang, S. Krystofova, and K.A. Borkovich. 2012. Roles for receptors, pheromones, G proteins, and mating type genes during sexual reproduction in *Neurospora crassa*. *Genetics*. 190:1389-1404.
- Köhler, J.R., B. Hube, R. Puccia, A. Casadevall, and J.R. Perfect. 2017. Fungi that infect humans. *Microbiology Spectrum*. 5.
- Konopka, J.B., A. Casadevall, J.W. Taylor, J. Heitman, and L. Cowen. 2019. One Health: Fungal Pathogens of Humans, Animals, and Plants: Report on an American Academy of Microbiology Colloquium held in Washington, DC, on October 18, 2017.
- Kozubowski, L., K. Saito, J.M. Johnson, A.S. Howell, T.R. Zyla, and D.J. Lew. 2008. Symmetry-breaking polarization driven by a Cdc42p GEF-PAK complex. *Current biology : CB*. 18:1719-1726.
- Kuo, C.-C., N.S. Savage, H. Chen, C.-F. Wu, T.R. Zyla, and D.J. Lew. 2014. Inhibitory GEF phosphorylation provides negative feedback in the yeast polarity circuit. *Current biology : CB*. 24:753-759.
- Lakhani, V., and T.C. Elston. 2017. Testing the limits of gradient sensing. *PLoS Comput Biol*. 13:e1005386.
- Lee, S., W.A. Lim, and K.S. Thorn. 2013. Improved blue, green, and red fluorescent protein tagging vectors for *S. cerevisiae*. *PloS one*. 8:e67902.
- Lee, S.S., P. Horvath, S. Pelet, B. Hegemann, L.P. Lee, and M. Peter. 2012. Quantitative and dynamic assay of single cell chemotaxis. *Integr Biol (Camb)*. 4:381-390.
- Lesage, G., and H. Bussey. 2006. Cell wall assembly in *Saccharomyces cerevisiae*. *Microbiology and Molecular Biology Reviews*. 70:317-343.
- Levin, D.E. 2011. Regulation of cell wall biogenesis in *Saccharomyces cerevisiae*: The cell wall integrity signaling pathway. *Genetics*. 189:1145.

- Lew, D.J. 2003. The morphogenesis checkpoint: How yeast cells watch their figures. *Current Opinion in Cell Biology*. 15:648-653.
- Lin, X., C.M. Hull, and J. Heitman. 2005. Sexual reproduction between partners of the same mating type in *Cryptococcus neoformans*. *Nature*. 434:1017-1021.
- Longtine, M.S., A. McKenzie, 3rd, D.J. Demarini, N.G. Shah, A. Wach, A. Brachat, P. Philippsen, and J.R. Pringle. 1998. Additional modules for versatile and economical PCR-based gene deletion and modification in *Saccharomyces cerevisiae*. *Yeast (Chichester, England)*. 14:953-961.
- Madden, K., and M. Snyder. 1992. Specification of sites for polarized growth in *Saccharomyces cerevisiae* and the influence of external factors on site selection. *Molecular biology of the cell*. 3:1025-1035.
- Manney, T.R. 1983. Expression of the *BAR1* gene in *Saccharomyces cerevisiae*: Induction by the alpha mating pheromone of an activity associated with a secreted protein. *Journal of bacteriology*. 155:291-301.
- Martin, S.G. 2019. Molecular mechanisms of chemotropism and cell fusion in unicellular fungi. 132:jcs230706.
- McClure, A.W., K.C. Jacobs, T.R. Zyla, and D.J. Lew. 2018. Mating in wild yeast: Delayed interest in sex after spore germination. *Molecular biology of the cell*:mbcE18080528.
- McClure, Allison W., M. Minakova, Jayme M. Dyer, Trevin R. Zyla, Timothy C. Elston, and Daniel J. Lew. 2015. Role of polarized G protein signaling in tracking pheromone gradients. *Developmental cell*. 35:471-482.
- Merlini, L., O. Dudin, and S.G. Martin. 2013. Mate and fuse: How yeast cells do it. *Open Biology*. 3.
- Merlini, L., B. Khalili, F.O. Bendezu, D. Hurwitz, V. Vincenzetti, D. Vavylonis, and S.G. Martin. 2016. Local pheromone release from dynamic polarity sites underlies cell-cell pairing during yeast mating. *Current biology : CB*. 26:1117-1125.
- Michaelis, S., and J. Barrowman. 2012. Biogenesis of the *Saccharomyces cerevisiae* pheromone a-factor, from yeast mating to human disease. *Microbiology and molecular biology reviews : MMBR*. 76:626-651.

- Miyanaaga, Y., S. Matsuoka, T. Yanagida, and M. Ueda. 2007. Stochastic signal inputs for chemotactic response in *Dictyostelium* cells revealed by single molecule imaging techniques. *Biosystems*. 88:251-260.
- Moore, S.A. 1983. Comparison of dose-response curves for alpha factor-induced cell division arrest, agglutination, and projection formation of yeast cells. Implication for the mechanism of alpha factor action. *The Journal of biological chemistry*. 258:13849-13856.
- Moore, T.I., C.-S. Chou, Q. Nie, N.L. Jeon, and T.-M. Yi. 2008. Robust spatial sensing of mating pheromone gradients by yeast cells. *PloS one*. 3:e3865.
- Moore, T.I., H. Tanaka, H.J. Kim, N.L. Jeon, and T.-M. Yi. 2013. Yeast G-proteins mediate directional sensing and polarization behaviors in response to changes in pheromone gradient direction. 24:521-534.
- Moran, K.D., H. Kang, A.V. Araujo, T.R. Zyla, K. Saito, D. Tsygankov, and D.J. Lew. 2019. Cell-cycle control of cell polarity in yeast. *The Journal of cell biology*. 218:171-189.
- Morrow, C.A., and J.A. Fraser. 2009. Sexual reproduction and dimorphism in the pathogenic basidiomycetes. *FEMS Yeast Research*. 9:161-177.
- Moskow, J.J., A.S. Gladfelter, R.E. Lamson, P.M. Pryciak, and D.J. Lew. 2000. Role of Cdc42p in pheromone-stimulated signal transduction in *Saccharomyces cerevisiae*. *Molecular and cellular biology*. 20:7559-7571.
- Nadin-Davis, S.A., and A. Nasim. 1990. *Schizosaccharomyces pombe* ras1 and byr1 are functionally related genes of the ste family that affect starvation-induced transcription of mating-type genes. *Molecular and cellular biology*. 10:549-560.
- Nern, A., and R.A. Arkowitz. 1998. A GTP-exchange factor required for cell orientation. *Nature*. 391:195-198.
- Nern, A., and R.A. Arkowitz. 1999. A Cdc24p-Far1p-Gbetagamma protein complex required for yeast orientation during mating. *The Journal of cell biology*. 144:1187-1202.
- Nern, A., and R.A. Arkowitz. 2000. G proteins mediate changes in cell shape by stabilizing the axis of polarity. *Molecular cell*. 5:853-864.

- Nichols, J.M., D. Veltman, and R.R. Kay. 2015. Chemotaxis of a model organism: Progress with *Dictyostelium*. *Curr Opin Cell Biol.* 36:7-12.
- Ozoe, F., R. Kurokawa, Y. Kobayashi, H.T. Jeong, K. Tanaka, K. Sen, T. Nakagawa, H. Matsuda, and M. Kawamukai. 2002. The 14-3-3 proteins Rad24 and Rad25 negatively regulate Byr2 by affecting its localization in *Schizosaccharomyces pombe*. *Molecular and cellular biology.* 22:7105-7119.
- Paliwal, S., P.A. Iglesias, K. Campbell, Z. Hilioti, A. Groisman, and A. Levchenko. 2007. MAPK-mediated bimodal gene expression and adaptive gradient sensing in yeast. *Nature.* 446:46-51.
- Park, H.O., and E. Bi. 2007. Central roles of small GTPases in the development of cell polarity in yeast and beyond. *Microbiology and molecular biology reviews : MMBR.* 71:48-96.
- Pruyne, D., L. Gao, E. Bi, and A. Bretscher. 2004a. Stable and dynamic axes of polarity use distinct formin isoforms in budding yeast. *Molecular biology of the cell.* 15:4971-4989.
- Pruyne, D., A. Legesse-Miller, L. Gao, Y. Dong, and A. Bretscher. 2004b. Mechanisms of polarized growth and organelle segregation in yeast. *Annu Rev Cell Dev Biol.* 20:559-591.
- Pryciak, P.M., and F.A. Huntress. 1998. Membrane recruitment of the kinase cascade scaffold protein Ste5 by the Gbetagamma complex underlies activation of the yeast pheromone response pathway. *Genes & development.* 12:2684-2697.
- Rappaport, N., and N. Barkai. 2012. Disentangling signaling gradients generated by equivalent sources. *Journal of Biological Physics.* 38:267-278.
- Rasmann, S., A. Bennett, A. Biere, A. Karley, and E. Guerrieri. 2017. Root symbionts: Powerful drivers of plant above- and belowground indirect defenses. *Insect Science.* 24:947-960.
- Raths, S.K., F. Naider, and J.M. Becker. 1988. Peptide analogues compete with the binding of alpha-factor to its receptor in *Saccharomyces cerevisiae*. *The Journal of biological chemistry.* 263:17333-17341.
- Robertson, C.G., M.R. Clark-Cotton, and D.J. Lew. in press. Mechanisms that ensure monogamous mating in *Saccharomyces cerevisiae*. *Molecular biology of the cell:mbc.*E20-12-0757.

- Roca, M.G., J. Arlt, C.E. Jeffree, and N.D. Read. 2005. Cell biology of conidial anastomosis tubes in *Neurospora crassa*. *Eukaryotic cell*. 4:911-919.
- Rogers, D.W., E. McConnell, and D. Greig. 2012. Molecular quantification of *Saccharomyces cerevisiae* α -pheromone secretion. *FEMS Yeast Res*. 12:668-674.
- Sarris, M., and M. Sixt. 2015. Navigating in tissue mazes: Chemoattractant interpretation in complex environments. *Current Opinion in Cell Biology*. 36:93-102.
- Schenkman, L.R., C. Caruso, N. Pagé, and J.R. Pringle. 2002. The role of cell cycle-regulated expression in the localization of spatial landmark proteins in yeast. *The Journal of cell biology*. 156:829-841.
- Segall, J.E. 1993. Polarization of yeast cells in spatial gradients of alpha mating factor. *Proceedings of the National Academy of Sciences of the United States of America*. 90:8332-8336.
- Simon, M.N., C. De Virgilio, B. Souza, J.R. Pringle, A. Abo, and S.I. Reed. 1995. Role for the Rho-family GTPase Cdc42 in yeast mating-pheromone signal pathway. *Nature*. 376:702-705.
- Sloat, B.F., A. Adams, and J.R. Pringle. 1981. Roles of the CDC24 gene product in cellular morphogenesis during the *Saccharomyces cerevisiae* cell cycle. *The Journal of cell biology*. 89:395-405.
- Smith, S.E., and D.J. Read. 2008. Mycorrhizal Symbiosis. Elsevier Science & Technology, San Diego, UNITED KINGDOM.
- Strickfaden, S.C., and P.M. Pryciak. 2008. Distinct roles for two Galpha-Gbeta interfaces in cell polarity control by a yeast heterotrimeric G protein. *Molecular biology of the cell*. 19:181-197.
- Suchkov, D.V., R. DeFlorio, E. Draper, A. Ismael, M. Sukumar, R. Arkowitz, and D.E. Stone. 2010. Polarization of the yeast pheromone receptor requires its internalization but not actin-dependent secretion. *Molecular biology of the cell*. 21:1737-1752.
- Swaney, K.F., C.H. Huang, and P.N. Devreotes. 2010. Eukaryotic chemotaxis: A network of signaling pathways controls motility, directional sensing, and polarity. *Annual review of biophysics*. 39:265-289.

- Taxis, C., P. Keller, Z. Kavagiou, L.J. Jensen, J. Colombelli, P. Bork, E.H.K. Stelzer, and M. Knop. 2005. Spore number control and breeding in *Saccharomyces cerevisiae*: A key role for a self-organizing system. *The Journal of cell biology*. 171:627-640.
- Taxis, C., and M. Knop. 2006. System of centromeric, episomal, and integrative vectors based on drug resistance markers for *Saccharomyces cerevisiae*. *BioTechniques*. 40:73-78.
- Tedersoo, L., M. Bahram, and M. Zobel. 2020. How mycorrhizal associations drive plant population and community biology. *Science*. 367:eaba1223.
- Valtz, N., M. Peter, and I. Herskowitz. 1995. FAR1 is required for oriented polarization of yeast cells in response to mating pheromones. *The Journal of cell biology*. 131:863-873.
- Vasen, G., P. Dunayevich, and A. Colman-Lerner. 2020a. Mitotic and pheromone-specific intrinsic polarization cues interfere with gradient sensing in *Saccharomyces cerevisiae*. *Proceedings of the National Academy of Sciences*. 117:6580.
- Vasen, G., P. Dunayevich, A. Constantinou, and A. Colman-Lerner. 2020b. GPCR receptor phosphorylation and endocytosis are not necessary to switch polarized growth between internal cues during pheromone response in *S. cerevisiae*. *Communicative & Integrative Biology*. 13:128-139.
- Wallen, R.M., and M.H. Perlin. 2018. An overview of the function and maintenance of sexual reproduction in dikaryotic fungi. *Front Microbiol*. 9:503.
- Wang, P., J.R. Perfect, and J. Heitman. 2000. The G-protein β Subunit GPB1 is required for mating and haploid fruiting in *Cryptococcus neoformans*. *Molecular and cellular biology*. 20:352-362.
- Wang, X., W. Tian, B.T. Banh, B.-M. Statler, J. Liang, and D.E. Stone. 2019. Mating yeast cells use an intrinsic polarity site to assemble a pheromone-gradient tracking machine. *The Journal of cell biology*:jcb.201901155.
- Wang, Y., H.P. Xu, M. Riggs, L. Rodgers, and M. Wigler. 1991. *byr2*, a *Schizosaccharomyces pombe* gene encoding a protein kinase capable of partial suppression of the *ras1* mutant phenotype. *Molecular and cellular biology*. 11:3554-3563.
- Woods, B., C.-C. Kuo, C.-F. Wu, T.R. Zyla, and D.J. Lew. 2015. Polarity establishment requires localized activation of Cdc42. *The Journal of cell biology*. 211:19-26.

- Wright, G.D., J. Arlt, W.C.K. Poon, and N.D. Read. 2007. Optical tweezer micromanipulation of filamentous fungi. *Fungal Genetics and Biology*. 44:1-13.
- Wu, C.F., J.G. Chiou, M. Minakova, B. Woods, D. Tsygankov, T.R. Zyla, N.S. Savage, T.C. Elston, and D.J. Lew. 2015. Role of competition between polarity sites in establishing a unique front. *Elife*. 4.
- Yi, T.M., H. Kitano, and M.I. Simon. 2003. A quantitative characterization of the yeast heterotrimeric G protein cycle. *Proceedings of the National Academy of Sciences of the United States of America*. 100:10764-10769.
- Zhao, Y., J. Lin, Y. Fan, and X. Lin. 2019. Life cycle of *Cryptococcus neoformans*. *Annual Review of Microbiology*. 73:17-42.
- Zhao, Z.S., T. Leung, E. Manser, and L. Lim. 1995. Pheromone signalling in *Saccharomyces cerevisiae* requires the small GTP-binding protein Cdc42p and its activator CDC24. *Molecular and cellular biology*. 15:5246-5257.

Biography

Manuella R. Clark-Cotton earned a B.S. (biology, Millsaps College, 1994), M.A. (applied linguistics, Boston University, 2003), and M.S. (biological sciences, Mississippi State University, 2012). In 2014 she joined the Duke University Program in Cell and Molecular Biology and affiliated with the Department of Cell Biology. She was an HHMI Gilliam Fellow (2016-9), BWF Graduate Diversity Program awardee (2017-9), and president of the Bouchet Society (2017-9).

Clark-Cotton MR, Henderson NT, Pablo M, Ghose D, Elston TC & Lew DJ. Exploratory polarization facilitates mating partner selection in *Saccharomyces cerevisiae*. *Mol Biol Cell* (in press).

Robertson CG, Clark-Cotton MR & Lew DJ. Mechanisms that ensure monogamous mating in *Saccharomyces cerevisiae*. *Mol Biol Cell* (in press).

Henderson NT, Pablo M, Ghose D, Clark-Cotton MR, Nolen J, Elston TC & Lew DJ. Ratiometric GPCR signaling enables directional sensing in yeast. *PLoS Biology*, 17(10): e3000484.

Goral M, Clark-Cotton M, Spiro A, Obler LK, Verkuilen J & Albert ML. The contribution of set switching and working memory to sentence comprehension in older adults. *Experimental Aging Research*, Oct 37(5):516-38, 2011.

Obler LK, Rykhlevskaia E, Schnyer D, Clark-Cotton MR, Spiro A, Hyun J, Kim DS, Goral M & Albert ML. Bilateral brain regions associated with naming in older adults. *Brain and Language*, Jun 113(3):113-23, 2010.

Clark-Cotton MR, Goral M, Williams RK & Obler LK. Language and communication in aging. In *Encyclopedia of Gerontology*, 2nd edition, J. Birren (Ed.). Elsevier: London, 2007.

Goral M, Clark-Cotton MR & Albert ML. Language disorders: General. In *Encyclopedia of Gerontology*, 2nd edition, J. Birren (Ed.). Elsevier: London, 2007.

Brugos A, Clark-Cotton MR & Ha S (Eds.). *BUCLD 29: Proceedings of the 29th Annual Boston University Conference on Language Development and Online Supplement*, Cascadilla Press: Somerville, MA, 2005.